Toward a Measurement of the Cosmological Geometry at $z \sim 2$: Predicting Lyα Forest Correlation in Three Dimensions, and the Potential of Future Data Sets

Patrick McDonald [1]

ABSTRACT

The correlation between Lyα absorption in the spectra of quasar pairs can be used to measure the transverse distance scale at $z \sim 2$, which is sensitive to the cosmological constant (Ω_Λ) or other forms of vacuum energy. Using Hydro-PM simulations, I compute the three-dimensional power spectrum of the Lyα forest flux, $P_F(\mathbf{k})$, from which the redshift-space anisotropy of the correlation can be obtained. I find that box size $\sim 40\,h^{-1}\,\mathrm{Mpc}$ and resolution $\sim 40\,h^{-1}\,\mathrm{kpc}$ are necessary for convergence of the calculations to $\lesssim 5\%$ on all relevant scales, although somewhat poorer resolution can be used for large scales. I compute directly the linear theory bias parameters of the Lyα forest, potentially allowing simulation results to be extended to arbitrarily large scales. I investigate the dependence of $P_F(\mathbf{k})$ on the primordial power spectrum, the temperature-density relation of the gas, and the mean flux decrement, finding that the redshift-space anisotropy is relatively insensitive to these parameters. A table of results is provided for different parameter variations. I investigate the constraint that can be obtained on Ω_Λ using quasars from a large survey. Assuming $13\,(\theta/1')^2$ pairs at separation $< \theta$, and including separations $< 10'$, a measurement to $\lesssim 5\%$ can be made if simulations can predict the redshift-space anisotropy with $\lesssim 5\%$ accuracy, or to $\lesssim 10\%$ if the anisotropy must be measured from the data. The Sloan Digital Sky Survey (SDSS) will obtain spectra for a factor ~ 5 fewer pairs than this, so followup observations of fainter pair candidates will be necessary. I discuss the requirements on spectral resolution and signal-to-noise ratio (SDSS quality spectra are sufficient).

Subject headings: cosmology: theory—intergalactic medium—large-scale structure of universe—methods: N-body simulations—quasars: absorption lines

1. INTRODUCTION

The theory of the Lyα forest based on gravitational collapse of a continuously fluctuating intergalactic medium (IGM) has been used to account for the correlation in absorption along the

---

[1]Department of Astronomy, The Ohio State University, Columbus, OH 43210; mcdonald@astronomy.ohio-state.edu

line of sight to single quasars, and to infer from these observations the primordial power spectrum of density perturbations (Croft et al. 1999, 2000; McDonald et al. 2000). Now the calculation should be extended to correlation across the line of sight, i.e., correlation between absorption in spectra of quasars separated by small angles in the sky. Comparison of theoretical predictions to a measurement of the full dependence of the correlation function of the transmitted flux on angle and separation will be a valuable test of the Lyα forest theory itself; however, the ultimate purpose of this measurement is to constrain the cosmological geometry at $z \sim 2$ through the Alcock & Paczyński (1979) test (hereafter, AP test), as proposed by McDonald & Miralda-Escudé (1999) and Hui, Stebbins, & Burles (1999). The AP test is in turn sensitive to the presence of a cosmological constant, Ω_Λ, or other kinds of vacuum energy. This paper addresses the need to understand the redshift-space anisotropy of the Lyα forest correlation in order to perform an accurate measurement of cosmological parameters.

We can move aggressively to use the Lyα forest as a cosmological probe because a working theory for the formation of the forest has been developed in many papers over the last decade, using semi-analytic methods and numerical simulations (e.g., McGill 1990; Bi 1993; Cen et al. 1994; Zhang, Anninos, & Norman 1995; Petitjean, Mücket, & Kates 1995; Hernquist et al. 1996; Miralda-Escudé et al. 1996; Hui, Gnedin, & Zhang 1997; Gnedin & Hui 1998; Theuns et al. 1998). The theory has been tested by comparing predictions with observed statistics of fitted absorption lines and the transmitted flux itself (e.g., Bechtold et al. 1994; Dinshaw et al. 1994; Rauch et al. 1997; Davé et al. 1997; Gnedin 1998; Crotts & Fang 1998; Theuns et al. 1999; McDonald et al. 2000; Zaldarriaga, Seljak, & Hui 2000).

In this primarily theoretical paper, I present computations of the three-dimensional power spectrum of the transmitted flux (equivalent to the correlation function). The flux power on large scales is given by the usual redshift-space formula derived from the linear theory of gravitational collapse (Kaiser 1987):

$$P_{F,L}(\mathbf{k}) = b^2(1 + \beta\mu^2)^2 P_L(k) , \tag{1}$$

where $\mathbf{k}$ is the redshift-space wavenumber, $P_L(k)$ is the real-space, linear theory power at $k \equiv |\mathbf{k}|$, $\mu = k_\parallel/k$, $k_\parallel$ is the projection of $\mathbf{k}$ along the line of sight, b is a "bias" parameter relating flux fluctuations to density fluctuations, and β is a second parameter describing the redshift-space anisotropy. I compute the values of both of these parameters from the Lyα forest theory using numerical simulations. [Usually, b and β have been discussed in the context of galaxy clustering, where $\beta \simeq \Omega_m^{0.6}(z)/b$ and $\Omega_m(z)$ is the matter density (in units of the critical density) at redshift z; however, for the Lyα forest β is an independent parameter (McDonald et al. 2000).] On small scales, where equation (1) is invalid because of non-linear effects, I extract the power spectrum from the simulations directly.

A direct computation of the bias parameters is unprecedented. While b and β set the amplitude of the large-scale (i.e., linear) power, their values are in fact determined by the small-scale structure of the field in question (i.e., transmitted flux or galaxy density), so the problem of computing their values from first principles is generally non-linear (see Dekel & Lahav 1998). In the case of the

galaxy density, a complete calculation is hopeless, because of the importance of star formation to galaxy formation, although some understanding of the physical nature and evolution of galaxy bias has been achieved by combining numerical simulations with semi-analytic prescriptions for star formation (e.g., Blanton et al. 2000; Benson et al. 2000; Cen & Ostriker 2000; Somerville et al. 2001). However, the Lya forest is much simpler according to the picture developed in the papers listed previously. We can simulate the small-scale structure in most of the volume of the IGM, essentially from first principles, and thus compute model predictions for any observable statistic of the Lyα forest transmitted flux, including the large-scale bias!

The observational motivation for this work is the impending flood of quasar spectra that will need to be analyzed in the near future [e.g., from the Sloan Digital Sky Survey (SDSS); York et al. 2000]. If their full potential for measuring Ω_Λ through the AP test (and also for measuring other parameters through the measurement of the small-scale power spectrum) is to be exploited, the accuracy of our model predictions must exceed the level currently used for one-dimensional work (e.g., Croft et al. 2000; Zaldarriaga, Hui, & Tegmark 2000). Here I take some first steps toward an accurate analysis of large data sets that include close pairs and groups of spectra. I examine some of the modeling uncertainties that have been under-studied in recent work focussed on interpreting one-dimensional data, including the effect of pressure in the simulations, the resolution and box size of the simulations, and the detailed dependence of the power spectrum on model parameters. I attempt to present the results in a form that will encourage comparison with other model predictions, and shed some light on the issues that need to be considered when planning the massive numerical studies that are inevitably needed before the results of a precision AP measurement can be believed (this paper can be thought of as a pilot study). Although I focus on the three-dimensional correlation needed to accomplish the AP test, many of the issues discussed are also relevant to the estimation of the mass power spectrum from one-dimensional data. Finally, I use the computed power spectrum to estimate the potential of the AP test to constrain Ω_Λ and the requirements on signal-to-noise (S/N) and resolution of the data, more realistically than previously possible.

The plan of the paper is as follows: In §2 I review the basics of the AP test. In §3 I describe and test my procedure for computing the power spectrum from simulations given a single set of model parameters. In §4 I describe the changes in the predicted power when each of the model parameters is varied. In §5 I discuss the AP test using my new power spectrum calculations. The reader who is interested first in cosmology, but not the details of the Lyα forest power spectrum, may want to read sections 3–5 in reverse order.

2. MEASURING THE COSMOLOGICAL GEOMETRY USING THE AP TEST

The function of redshift that relates angular separation ($\Delta\theta$) on the sky to Hubble flow velocity separation perpendicular to the line of sight ($\Delta v_\perp$) can be measured from the correlation function of any observable field by requiring that the correlation be isotropic in real space. At high redshift this

measurement is sensitive to the cosmological constant (Alcock & Paczyński 1979). One advantage of this method is the fact that no assumption of standard candles or rods is required, and it is therefore independent of evolutionary effects of observed "objects". The total velocity separation between two points along the line of sight is $\Delta v_\parallel = c\Delta z/(1+z) = \Delta v_h + \Delta v_p$ where Δz is the redshift separation, v_h is the Hubble flow velocity and v_p is the peculiar velocity. The perpendicular velocity separation is $\Delta v_\perp \equiv cf(z)\Delta\theta$, where $f(z) = c^{-1}H(z)D_A(z)$, $H(z)$ is the Hubble constant at z, and $D_A(z)$ is the usual angular diameter distance. With the assumption of isotropy, the real space two-point correlation function of fluctuations, $\xi_r(\Delta v_h, \Delta v_\perp)$, must be a function of $(\Delta v_h^2 + \Delta v_\perp^2)^{1/2}$ only. If ξ_r could be measured, it would be a relatively straightforward matter to measure $f(z)$ by simply demanding isotropy. However, generally the large-scale correlations in the universe are induced by gravitational collapse, and the peculiar velocities make the correlation function in redshift space anisotropic (Kaiser 1987). The peculiar velocities introduce an anisotropy in the observable (redshift space) correlation function, $\xi(\Delta v_p, \Delta v_\perp)$, of the same order as the difference in $f(z)$ between various cosmological models. In McDonald and Miralda-Escudé (1999) (see also Hui, Stebbins, & Burles 1999) we showed that it is possible to disentangle the effects of geometry and peculiar velocities and recover the desired global parameters from the correlations in the Lyα forest absorption.

I now show the sensitivity of $f(z)$ to cosmological parameters, assuming a model containing pressureless matter with density $\rho_m = \Omega_m \rho_c$, and a second component with negative pressure, $p = \omega \rho_\Lambda$, and energy density $\rho_\Lambda = \Omega_\Lambda \rho_c$, where ρ_c is the critical density. For simplicity, I assume ω is a constant. $f(z)$ is given by

$$f(z) = \frac{E(z)\ \mathrm{S}\left[\sqrt{\Omega_K}\int_0^z (dz'/E(z'))\right]}{(1+z)\sqrt{\Omega_K}}\ , \tag{2}$$

where $\mathrm{S}(x) \equiv x$ for a flat model ($\Omega_m + \Omega_\Lambda = 1$), $\mathrm{S}(x) \equiv \sinh x$ for an open model ($\Omega_m + \Omega_\Lambda < 1$), $\mathrm{S}(x) \equiv \sin x$ for a closed model ($\Omega_m + \Omega_\Lambda > 1$), $\Omega_K = |1 - \Omega_m - \Omega_\Lambda|$, and $E(z) = \left[\Omega_m (1+z)^3 + \Omega_K (1+z)^2 + \Omega_\Lambda (1+z)^{3(1+\omega)}\right]^{1/2}$. The redshift evolution of $f(z)$ in representative models is shown in Figure 1 (normalized by the value in an Einstein-de Sitter model with $\Omega_m = 1$ and $\Omega_\Lambda = 0$). This figure shows that the AP test is a much more efficient method of measuring Ω_m in a universe with a significant cosmological constant than in an open universe, with only pressureless matter. In the flat case, we see that the sensitivity of f to Ω_Λ peaks just beyond $z = 1$, and is fairly constant with increasing redshift.

In §5 I show that the effective central redshift for the Lyα forest AP test using SDSS data will be $z \simeq 2.25$, so I look more carefully at the sensitivity to parameters of $f(z)$ at this redshift. Figure 2 shows contours of constant $f(z = 2.25)$ in the Ω_m–Ω_Λ plane, assuming $\omega = -1$. For a typical model with $\Omega_m \simeq 0.3$ and $\Omega_\Lambda \simeq 0.7$, the contours are perpendicular to the line that indicates flatness. This means that a measurement of f complements the CMB anisotropy measurements, which constrain $\Omega_m + \Omega_\Lambda$, and will be a cross-check on the type Ia supernova measurements, which have contours similar to the Lyα forest test (recent CMB and SNIa constraints are combined in de Bernardis et al. 2000, and Balbi et al. 2000). Assuming the universe is flat, Figure 3 shows contours
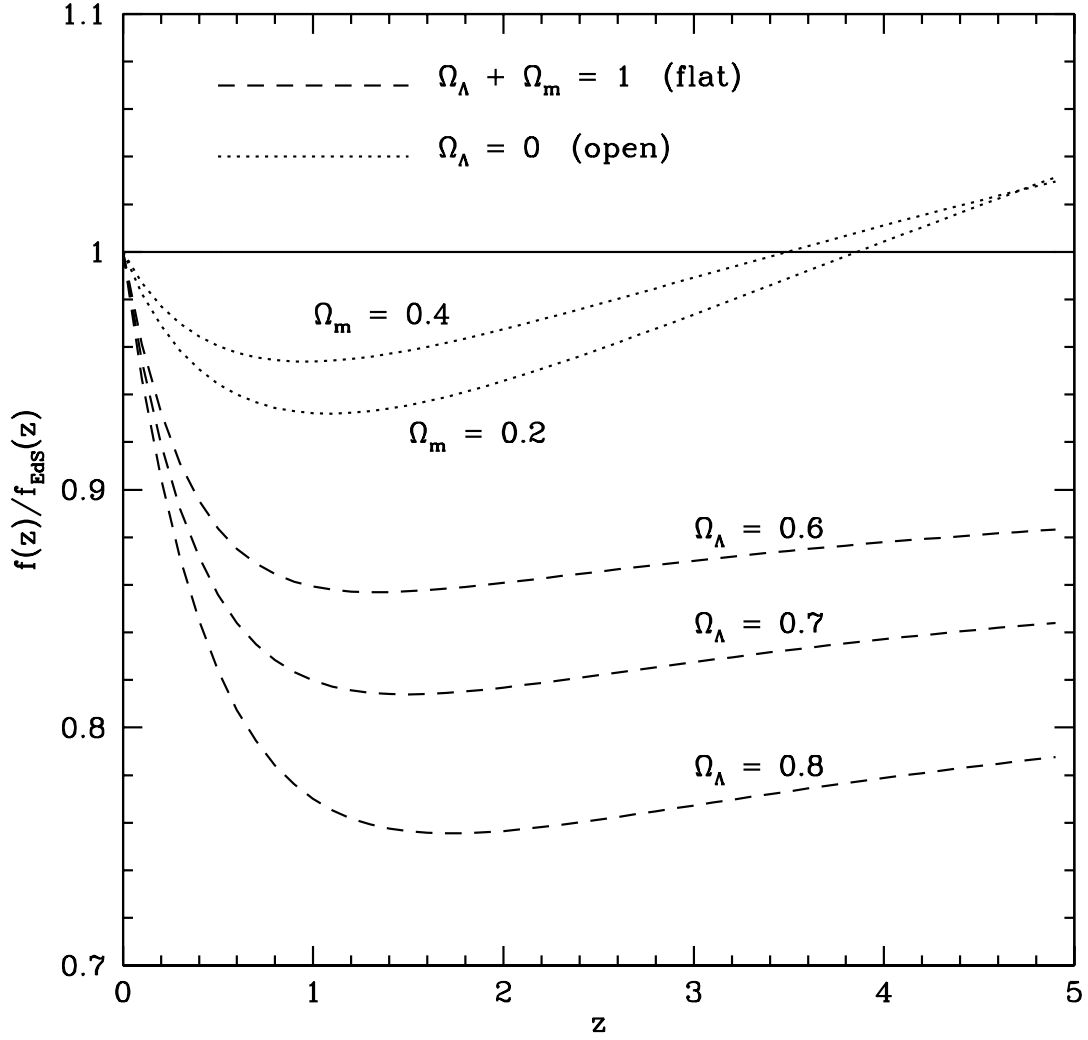
Fig. 1.— Redshift evolution of $f(z)$, relative to an Einstein-de Sitter model. The *dashed lines* show flat models (with $\omega = -1$), while the *dotted lines* show open models.
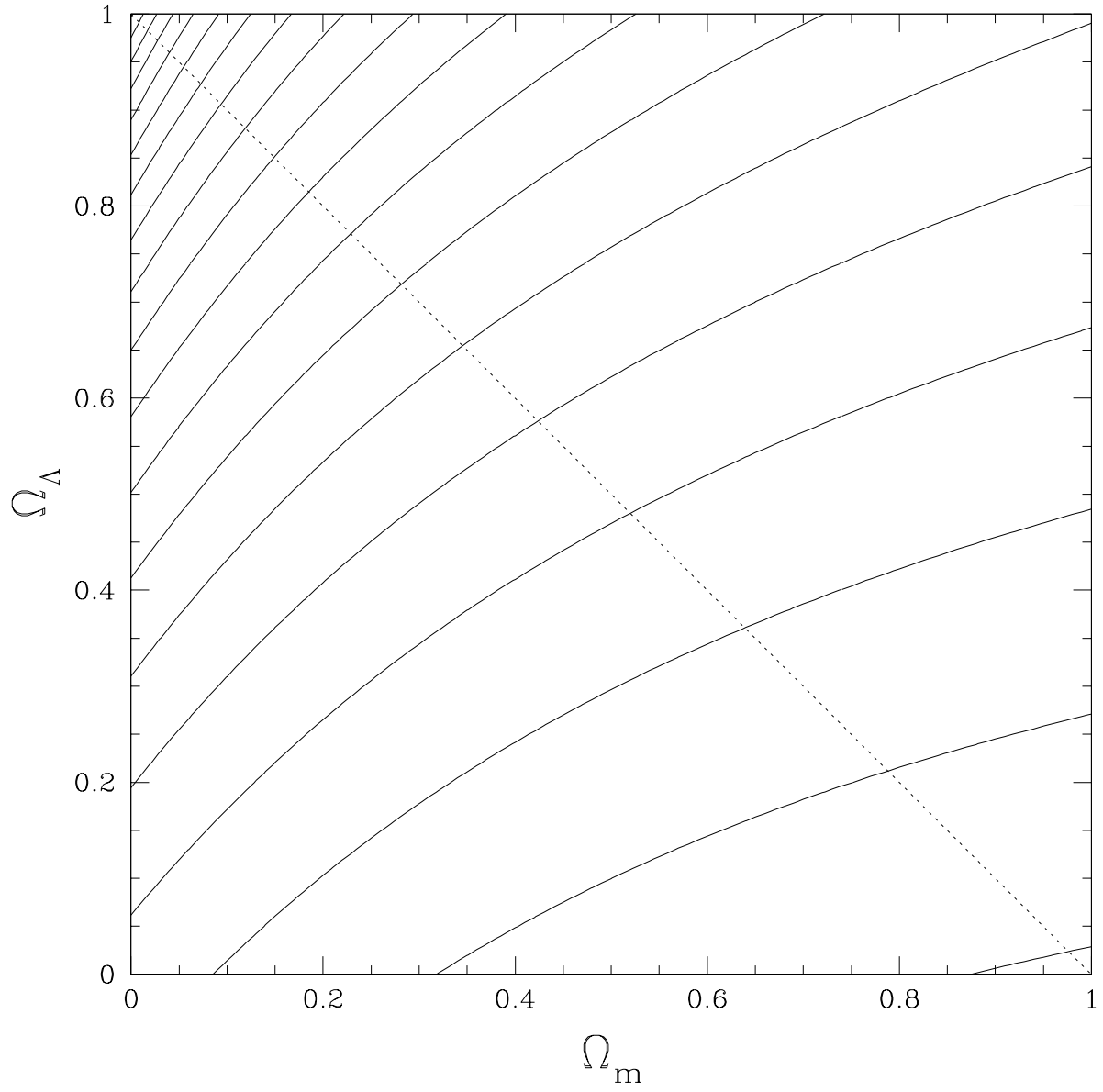
Fig. 2.— *solid lines*: contours of constant $f(z)$ (separated by 0.05), assuming $\omega = -1$. *dotted line*: $\Omega_m + \Omega_\Lambda = 1$.

of constant f in the Ω_m–ω plane. The remarkable insensitivity of the Lyα forest AP test to ω in models with $\omega \lesssim -0.5$ is actually a positive aspect of the test, because many of the other future tests (e.g., improved CMB, SNIa, and galaxy number counts) have roughly diagonal degeneracy contours in the Ω_m–ω plane (Huterer & Turner 2000).

Aside from measuring cosmological parameters, simply measuring $f(z)$ at high redshift would test the correctness of currently studied Friedmann-Robertson-Walker cosmological models in a qualitatively new regime.

3. COMPUTING THE THREE-DIMENSIONAL FLUX POWER SPECTRUM

The purpose of this section is to establish how I compute the three-dimensional flux power spectrum, $P_F(\mathbf{k})$, for a given set of model parameters, and to explore some of the potential numerical and modeling uncertainties. In §3.1 I describe the simulations that I use, in §3.2 I investigate the effect of pressure in the simulations, in §3.3 I test the effects of simulation resolution and box size, in §3.4 I introduce a method for extending the simulation predictions to scales larger than the box size by computing the linear theory bias parameters for the Lyα forest, and in §3.5 I introduce a simple analytic fitting formula that conveniently describes the power for all $\mathbf{k}$.

When I discuss the modeling uncertainties, I will generally define better than 10% accuracy in the ratio of the power along to the power across the line of sight to be a "good" result. The anisotropy of the power is the most relevant quantity for the AP test. In §5 I show that 10% accuracy is more than sufficient to interpret existing data, and data that will exist in the very near future, and is approaching the accuracy needed for comparison with the full quasar sample of the SDSS. Furthermore, the approximations made in the Hydro-PM simulations that I use (described below) are only accurate to $\sim 10\%$, so this represents a lower limit on the achievable accuracy. Achieving better accuracy should be a straightforward matter of extending the type of study I present in this paper to include larger and fully hydrodynamic simulations.

For the reasons discussed in Hui et al. (2000), I compute the power in the fluctuations of $\delta_F(\mathbf{x}) \equiv F(\mathbf{x})/\bar{F} - 1$, where $\bar{F}$ is the mean transmitted flux, and $\mathbf{x}$ is the redshift-space coordinate (i.e., the component of $\mathbf{x}$ along the line of sight is $\Delta v_\parallel$, while the components transverse to the line of sight are described by $\Delta v_\perp$ and an azimuthal angle). I use the normalization convention

$$\langle \delta_F^2 \rangle = \int \frac{d^3\mathbf{k}}{(2\pi)^3} P_F(\mathbf{k}) \ , \tag{3}$$

so the flux correlation function is

$$\xi_F(\mathbf{x}) = \langle \delta_F(\mathbf{r}) \, \delta_F(\mathbf{r} + \mathbf{x}) \rangle = \int \frac{d^3\mathbf{k}}{(2\pi)^3} P_F(\mathbf{k}) \ \exp(-i\mathbf{k} \cdot \mathbf{x}) \ . \tag{4}$$

For convenience, I sometimes plot the quantity

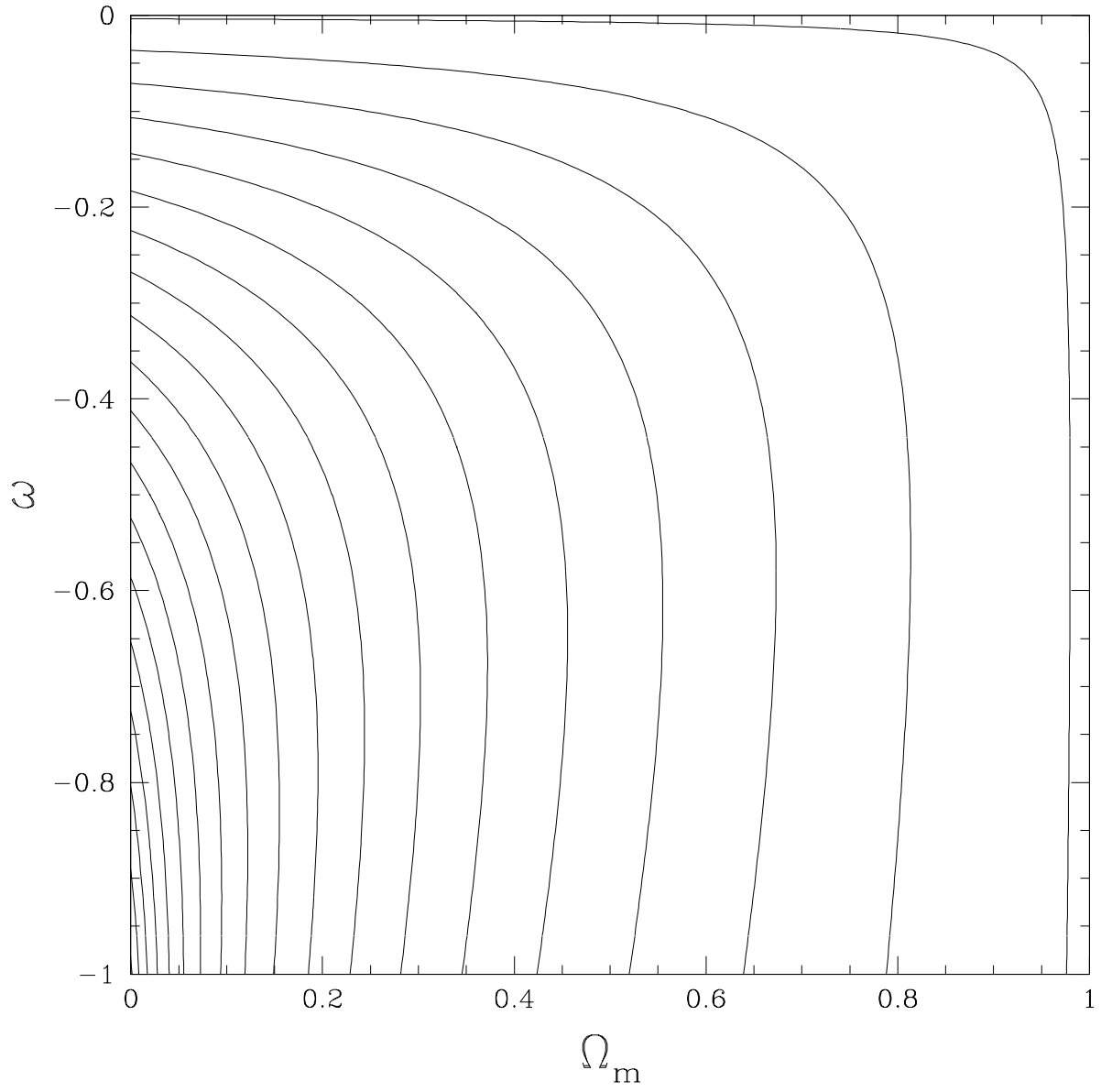$$\Delta_F^2(\mathbf{k}) \equiv \frac{k^3}{2\pi^2} P_F(\mathbf{k}) \ , \tag{5}$$

Fig. 3.— Contours of constant $f(z)$ (separated by 0.05), assuming a flat universe ($\Omega_m + \Omega_\Lambda = 1$).

where $k \equiv |\mathbf{k}|$. I use $\mu \equiv k_\parallel/k$ to describe the angle between the wavevector $\mathbf{k}$ and the line of sight, where $k_\parallel$ is the component of $\mathbf{k}$ along the line of sight.

Before we dive into detailed figures showing the Lyα forest power spectrum, it is helpful to see its place in the context of cold dark matter (CDM) models. Figure 4 compares $P_F(\mathbf{k})$ (at $z = 2$) to the linear and non-linear power spectra of the mass fluctuations (in real space). The linear (thick solid line) and non-linear (thick dotted line) power are from the fitting formulas given by Ma (1998). The cosmological model is flat ΛCDM at $z = 2$, with $\sigma_8 = 0.79$, $n = 0.95$, $\Omega_m = 0.4$, and $h = 0.65$. The flux power is from the analytic fitting formula described in §3.5, with $\mu = 1$ for the solid line, and $\mu = 0$ for the dotted line. The measurements by Croft et al. (1999), McDonald et al. (2000), and Croft et al. (2000) of the mass power from the one-dimensional flux power were most sensitive to power at the wavenumbers indicated by short, vertical lines in Figure 4: $k = 0.96\ (h^{-1}\,\mathrm{Mpc})^{-1}$, $k = 5.1\ (h^{-1}\,\mathrm{Mpc})^{-1}$, and $k = 3.7\ (h^{-1}\,\mathrm{Mpc})^{-1}$, respectively (for my assumed cosmological model, note that the vertical position of these lines is *meaningless*). To show the unique usefulness of the Lyα forest to constrain small scale fluctuations, I also plot (*points with error bars*) the galaxy power spectrum at $z = 0$, in the linear regime, from Hamilton & Tegmark (2000), with an arbitrary rescaling of the amplitude to account for evolution to $z = 2$ and bias. (the galaxy clustering is measured also on smaller scales, but these results are difficult to interpret because of our inability to fully simulate the formation of galaxies)

Note that throughout this paper I plot figures with k measured in $(h^{-1}\,\mathrm{Mpc})^{-1}$ on the lower horizontal axis, and in $(\mathrm{km\,s^{-1}})^{-1}$ on the upper horizontal axis, transforming between the two using the model in the simulations; however, the reader should keep in mind that the observable coordinates are velocity along the line of sight, and angular separation transverse to the line of sight.

3.1. Description of the Numerical Simulations

In this subsection I discuss my procedure for computing the flux power spectrum, which breaks neatly into two parts: First, simulations using a given set of cosmological parameters (e.g., σ_8) and a given thermal history (temperature-density relation at all times) are evolved to give the baryon density and velocity fields, which are output at desired redshifts. Later, using these outputs, simulated spectra can be created for different choices of the parameters of the Lyα forest model (the temperature-density relation at the output time, and the normalization of the optical depth).

3.1.1. Density and Velocity Fields from HPM Simulations

For the purpose of this paper, the freedom to run many simulations quickly is more important than having the most realistic simulations possible. The Lyα forest is modeled using the Hydro-PM (HPM) approximation to evolve the baryon density and velocity fields, using the same code
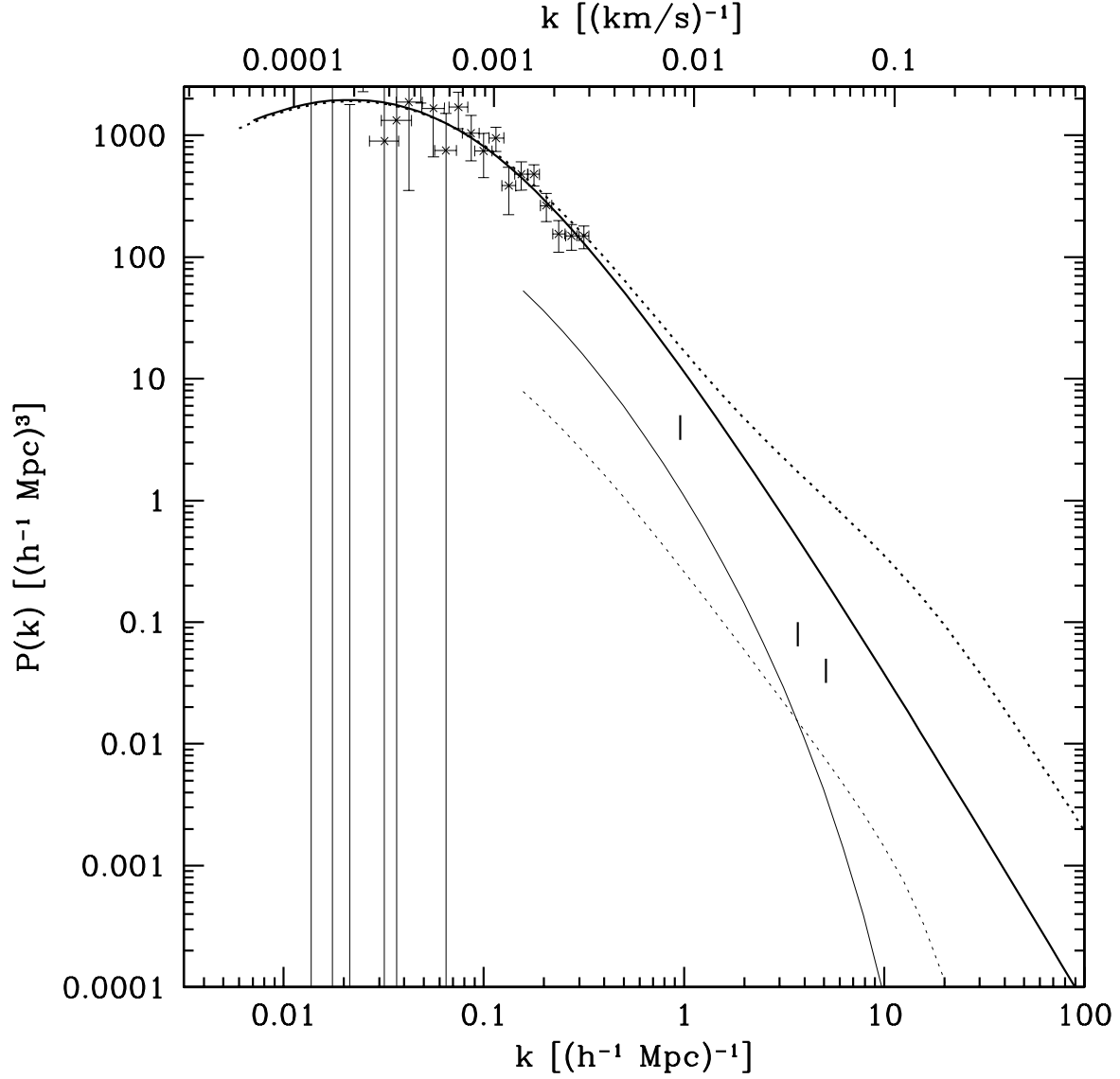
Fig. 4.— Lyα forest power vs. mass power and galaxy power. The *thin solid* and *thin dotted* lines show predictions for $P_F(\mathbf{k})$ along and across the line of sight, respectively, for a ΛCDM model at $z = 2$. The *thick solid* line shows the linear theory, real space power of the mass fluctuations, while the *thick dotted* line shows the non-linear mass power. Short, vertical lines indicate the central wavenumbers for several recent determinations of the mass power spectrum using the one-dimensional flux power (the vertical positions of these lines are completely arbitrary). Points with error bars show the $z = 0$ galaxy power spectrum in the linear regime, from Hamilton & Tegmark (2000) (arbitrarily rescaled in amplitude).

described in Gnedin & Hui (1998). One set of particles is used to represent both the baryons and dark matter. A pseudo-pressure term, based on an assumed temperature-density relation (equation 8 below), is added to the usual Newtonian force law as follows:

$$\frac{d\mathbf{v}}{dt} + H\mathbf{v} = -\nabla\phi - \frac{1}{\rho}\nabla P \equiv -\nabla\psi \; , \tag{6}$$

with

$$\psi = \phi + \frac{P(\rho)}{\rho} + \int_1^\rho \frac{P(\rho')}{\rho'}\frac{d\rho'}{\rho'} \; , \tag{7}$$

where $\mathbf{v}$ is the particle velocity, ϕ is the gravitational potential, and $P(\rho) \propto \rho^\gamma$ is the pressure.

To compute the pressure term, the HPM cod assumes a power-law temperature-density relation,

$$T = T_0 \Delta^{\gamma-1} \; , \tag{8}$$

where Δ is the density in units of the mean density. This form arises naturally for gas expanding adiabatically in ionization equilibrium with a background radiation field, where the temperature is set by photoionization heating and adiabatic cooling (Hui & Gnedin 1997). Fully hydrodynamic simulations confirm that equation (8) provides a reasonable approximate description of the temperature-density relation for $\Delta \lesssim 5-10$, above which shock heating leads to substantial dispersion in the temperatures at fixed densities (Croft et al. 1997; Theuns et al. 1998). Since most Lyα forest absorption is by gas with $\Delta < 5$, it is not too surprising that the HPM simulation method can give good agreement with the results of fully hydrodynamic simulations (Gnedin & Hui 1998). In practice, I usually use the parameter $T_{1.4} \equiv T_0 \, 1.4^{\gamma-1}$ in place of T_0, because McDonald et al. (2001) measured the temperature most precisely at $\Delta = 1.4$.

For the purpose of computing this pressure term only, the parameters of the temperature-density relation in my simulations are set to the measured values from McDonald et al. (2001): $T_{1.4}$=(20100, 20300, 20700) K, and $\gamma - 1$ =(0.43, 0.29, 0.52), at $\bar{z}$ =(3.9, 3.0, 2.4), with reionization assumed to take place suddenly at $z = 7$, when the gas is raised from zero temperature to a constant temperature $T = 25000$ K (i.e., $\gamma - 1 = 0$). I interpolate linearly between the given redshifts. As I discuss further below, within the bounds allowed by the current observational measurements of the temperature-density relation, the detailed thermal history used to evolve the simulation is not important to our power spectrum results, at the level of accuracy that we are interested in this paper. For this reason, when I vary the temperature-density relation used to compute the recombination coefficient and thermal broadening when creating spectra (see §3.1.2), I do not need to re-run the simulations with a different thermal history.

The mesh cells in my simulations are always equal in size to the spacing between particles. Interpolation from the particles to the mesh is performed using triangular-shaped clouds (hereafter TSC; Hockney & Eastwood 1988). I will refer to the length of the box along an axis as L, and the number of particles as N.

3.1.2. Simulated Spectra

After the evolution of a simulation is completed, I create simulated spectra from which I measure the power spectrum. Entire simulation boxes are converted into spectra by using each grid cell in a face of the box as the origin for a line of sight through the simulation cube, i.e., a spectral pixel is generated for every cell in the box (in practice, I under-sample the transverse directions by factors of 2 because this saves computer time and does not introduce any noticeable error). The power spectrum is then obtained by a three-dimensional FFT.

The first step in creating spectra is to convert the HPM particle positions and velocities into density and velocity fields on a grid. This is done using the same TSC interpolation and grid spacing that was used in the evolution of the simulation.

Next, the baryon density is converted to H I density, n_{HI}, by assuming the gas is in ionization equilibrium with a uniform ionizing background, i.e., $n_{HI} \propto T^{-0.7} \Delta^2 / \Gamma$, where Γ is the ionization rate, and T is the temperature of the gas [I use $\alpha(T) \propto T^{-0.7}$ for the recombination coefficient]. Assuming the temperature is given by equation (8), I obtain from n_{HI} the optical depth in each cell in real-space (i.e., before the effects of peculiar velocities and thermal broadening),

$$
\tau_R = \tau_0(z)\ \Delta^\beta = 1.41 \frac{(1+z)^6\ \left(\Omega_B h^2\right)^2}{T_4^{0.7}\ hE(z)\ \Gamma_{-12}(z)}\ \Delta^\beta\ ,
\tag{9}
$$

where $E(z) = H(z)/H_0 \simeq \Omega_m^{1/2}\ (1+z)^{3/2}$ (I use the exact version), $H(z)$ is the Hubble constant at redshift z, H_0 is the present Hubble constant, $h = H_0/(100\,\mathrm{km\,s^{-1}\,Mpc^{-1}})$, Ω_B is the baryon density in units of the critical density (at the present time), $T_4 = T_0/(10000\ \mathrm{K})$, $\Gamma_{-12}(z)$ is the photoionization rate of hydrogen in units of $10^{-12}\,\mathrm{s^{-1}}$, and $\beta = 2 - 0.7\,(\gamma - 1)$.

Finally, to construct the spectrum along each line of sight, I evaluate the integral

$$
\tau(x) = \int \tau_R(x')\ W\left[x - x' - v_\parallel\left(x'\right), T\left(x'\right)\right] dx'\ ,
\tag{10}
$$

where x and x' are periodic velocity coordinates labeling the cells in the simulation in real-space and redshift-space respectively, $T(x)$ and $v_\parallel(x)$ are respectively the temperature and the velocity along the line of sight of the gas at x,

$$
W\left(x, T\right) = \exp\left[-\frac{1}{2}\frac{x^2}{\sigma^2(T)}\right] / \left[2\pi\sigma^2(T)\right]^{1/2}\ ,
\tag{11}
$$

and $\sigma(T) = 9.1\,\mathrm{km\,s^{-1}}\,(T/10000\ \mathrm{K})^{1/2}$. In practice, the details of the numerical implementation of this integral may make some difference to my results (specifically the resolution test). I use redshift-space pixels identical in size to the real-space cells in the simulation. I account for the expansion or contraction of cells by translating each cell-edge in real-space into redshift-space using the average velocity of the cells that the edge separates. The optical depth contributed by each real-space cell is distributed to multiple redshift-space pixels based on its fractional overlap with each. The

different contributions to a redshift-space pixel are thermally broadened separately, based on the temperature of the originating real-space cells. The observable quantity is $F(x) = \exp\left[-\tau\left(x\right)\right]$.

Because the values of the parameters that combine to form τ_0 are uncertain, especially the value of Γ_{-12}, τ_0 is effectively an unknown parameter. The mean transmitted flux, $\bar{F}$, is more directly observable, so I use it as the independent parameter, determining τ_0 by requiring that $\bar{F}$ in the simulation has the specified value. Unless otherwise indicated, all comparisons between simulations are at fixed $\bar{F}$. Note that many of my conclusions may be sensitive to large changes in the value of $\bar{F}$ (because $\bar{F}$ sets the typical density to which the power spectrum is sensitive), so they should not be assumed to hold at redshifts where the mean flux is much higher or lower.

In summary, the Lyα forest in my model, for a given density and velocity field (determined by the cosmological model), is specified by three free parameters: $\bar{F}$, $T_{1.4}$, and $\gamma - 1$.

For the numerical tests in §3.2 and §3.3 I use a set of simulations originally created for comparison with the hydrodynamic simulation L10 in Miralda-Escudé et al. (1996). The outputs are at $z = 2$, with cosmological parameters $\sigma_8 = 0.79$, $n = 0.95$, $\Omega_m = 0.4$, $\Omega_\Lambda = 0.6$, $\Omega_B = 0.0355$, and $h = 0.65$, and Lyα forest parameters $\bar{F} = 0.818$, $T_{1.4} = 15517$ K, $\gamma - 1 = 0.49$. Starting with the box size test at the end of §3.3, and throughout the rest of the paper, I use a different set of simulations, output at $z = 2.25$, and change the Lyα forest model parameters to $\bar{F} = 0.8$, $T_{1.4} = 20000$ K, and $\gamma - 1 = 0.5$ [consistent with the temperature measurement in McDonald et al. (2001)]. I show in §5 that $z \simeq 2.25$ is approximately the redshift where the most data will be available to perform the AP test.

Throughout this paper I actually included deviations from equation (8) when I computed the recombination coefficient and thermal broadening for spectra, in order to facilitate a future comparison between HPM results and simulations like the fully hydrodynamic simulation referred to as L10 in Miralda-Escudé et al. (1996). I add to the specified power-law the deviation from a power-law found in that simulation, i.e., the temperature that I use at a point with overdensity Δ is $T = T_0\Delta^{\gamma-1} + \delta T(\Delta)$, where $\delta T(\Delta)$ was obtained from the hydro simulation (see McDonald et al. 2001, Figure 1). This additional term makes less than 6% difference in the flux power spectrum for $k < 10\ (h^{-1}\,\mathrm{Mpc})^{-1}$ [and $< 4\%$ for $k < 4\ (h^{-1}\,\mathrm{Mpc})^{-1}$]. To promote reproducibility, the values of $\delta T(\Delta)$ that I used are available on request.

3.2.   HPM vs. PM

Ideally, we would always use fully hydrodynamic simulations to model the Lyα forest, like the one used to simulate the one-dimensional power spectrum in McDonald et al. (2000). Unfortunately, these simulations are very expensive to run, leading Croft et al. (1999, 2000) and Zaldarriaga et al. (2000) to use simple particle-mesh (PM) simulations. In this paper, except for in part of this subsection, I use the intermediate HPM method [see McDonald & Miralda-Escudé (2001), Meiksin & White (2000), and Ricotti, Gnedin, & Shull (2000) for some tests and applications]. The only

difference between the HPM and PM simulations is the former include a simple calculation of pressure, based on an assumed temperature-density relation, as described above. The primary difference between the HPM and full-hydro techniques is the latter include a full calculation of the temperature evolution of every element of gas and they include shocks. The most important practical consequence of this difference is probably the more realistic values for the temperatures used to compute the recombination coefficient and thermal broadening for the gas.

Before I make detailed comparisons between power spectra under different modeling assumptions, I make one relevant observation about the realities of Lyα forest data analysis: McDonald et al. (2000) showed that $P_{F,1D}(k)$ is significantly influenced by the presence of metal lines if $k \gtrsim 0.1(\,\mathrm{km\,s^{-1}})^{-1}$. This means that any measurement of Lyα forest statistics that is sensitive to power on this scale is suspect. Therefore, when I discuss the simulation predictions, I will not be very concerned about the power in the simulations at $k \gtrsim 0.1$ $(\,\mathrm{km\,s^{-1}})^{-1}$ $[k \gtrsim 10$ $(\,h^{-1}\,\mathrm{Mpc})^{-1}]$.

We expect that the pressure in an HPM simulation will smooth the gas on small scales, relative to a PM simulation. For example, in linear theory, and assuming temperature evolution $T \propto (1+z)$, the suppression factor for a Fourier mode, $\delta(k)$, with wavenumber k can be calculated analytically: $\delta(k)/\delta_0(k) = 1/[1+(k/k_J)^2]$, where δ_0 is the amplitude the mode would have in absence of pressure, $k_J = a\sqrt{4\pi G\rho}/c_s$, a is the expansion factor and c_s is the sound speed of the gas (e.g., Gnedin & Hui 1998). Because the Lyα forest structure is not linear, and the thermal evolution is different from $T \propto (1+z)$, the above formula will not hold quantitatively in my simulations, but we should see the same general effect. In Figure 5 I compare the flux power spectra from HPM and PM simulations (with identical initial conditions, $L = 8.89\,h^{-1}\,\mathrm{Mpc}$, and $N = 256^3$), plotting the ratio of HPM to PM power as the thick, black line. Throughout this paper (except in Figure 4), power measured from simulations "along the line of sight" refers to a bin where $0.75 < \mu < 1.0$, while power "across the line of sight" refers to $0.0 < \mu < 0.25$. We see the expected suppression by pressure of small-scale power transverse to the line of sight (for reference, the ratio of HPM to PM power is well fit by $1.1\exp[-(kr)^2]$, where $r = 37\,h^{-1}\,\mathrm{kpc}$), but an increase in the power along the line of sight. This increase, which occurs at k values where the power is already strongly suppressed by non-linear peculiar velocities, is probably the result of suppression of small-scale power in the velocity field. Of course, the change in $P_F(\mathbf{k})$ caused by pressure differences for reasonable changes in the temperature near the measured value (see McDonald et al. 2001) is much smaller than the difference between PM and HPM simulations. For a 4000 K change in temperature, the change in $P_F(\mathbf{k})$ is less than 2% at $k < 8$ $(\,h^{-1}\,\mathrm{Mpc})^{-1}$, justifying the assumption I make later that the only significant effect of changing the temperature is to change the thermal broadening and recombination coefficient in the creation of spectra.

The effect of pressure on the power spectrum can, in principle, extend to all scales; however, we see that the influence of pressure on large-scale power is rather small. This bodes well for the general idea that we can substitute HPM approximations for fully hydrodynamic calculations, at least for measurements at relatively large separations. That is, if the difference in power between PM and HPM is only 10%, it seems unlikely that any inaccuracy in the HPM pressure relative to
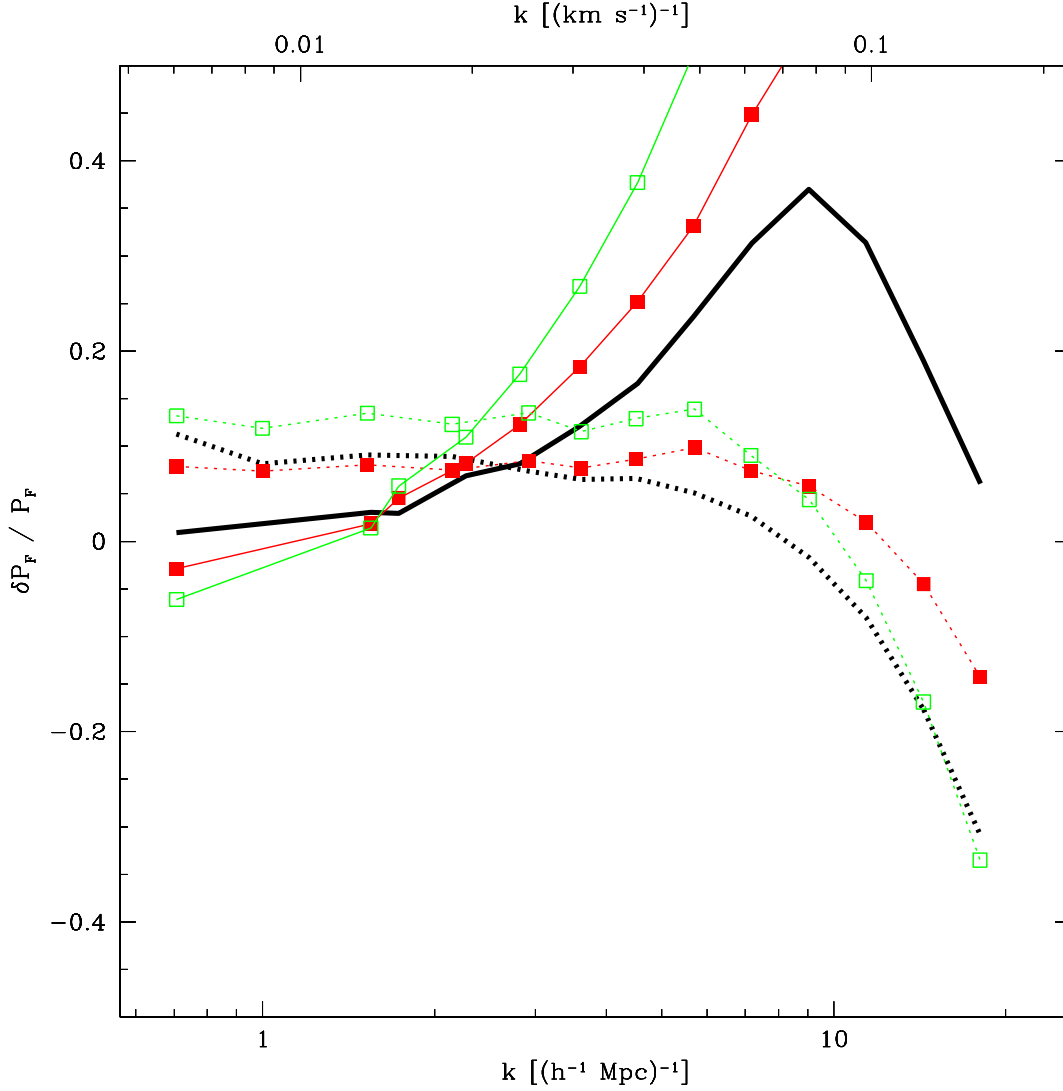
Fig. 5.— Fractional changes in power using different pressure approximation methods. All curves are relative to a simple PM simulation, and in all cases the *solid lines* show power along the line of sight $(0.75 < \mu < 1.0)$ and the *dotted lines* show power across the line of sight $(0.0 < \mu < 0.25)$. The *thick, black lines* show the difference between HPM and PM power. The squares connected by thin lines show Gaussian smoothing, $\exp[-(kr)^2/2]$, applied to the mass distribution, with $r = 35\,h^{-1}$ kpc (*red with filled squares*) and $r = 49\,h^{-1}$ kpc (*green with open squares*).

full-hydro will be significant (recall that $\sim 10\%$ accuracy in the ratio of power along to across the line of sight is roughly the level I am aiming for in this paper). The main outstanding difference between a full-hydro and an HPM simulation is the scatter in temperature at a single density, especially at high densities. A detailed test of the systematic differences between the two will be the subject of future work.

In their paper interpreting the observed one-dimensional flux power spectrum results of McDonald et al. (2000), Zaldarriaga et al. (2000) attempted to mimic the effect of pressure forces by smoothing the dark matter density in PM simulations before creating spectra. The lines highlighted by squares in Figure 5 show the results of this method for the three-dimensional power, where a Gaussian smoothing, $\exp[-(kr)^2/2]$, was applied to the mass density and momentum fields, using $r = 35\,h^{-1}\,\mathrm{kpc}$ (red line with filled squares) and $r = 49\,h^{-1}\,\mathrm{kpc}$ (green with open squares). While the results have a similar trend as the results from the HPM approximation, the relative strength of the effects in different regions of **k**-space are quantitatively different. Note also that Zaldarriaga et al. (2000) allowed r to be as high as $\sim 280\,h^{-1}\,\mathrm{kpc}$ – clearly much too high to give even a rough representation of pressure for a reasonable thermal history of the gas.

3.3.   Simulation Resolution and Box Size

To make accurate power spectrum predictions, it is necessary to be sure we sufficiently resolve the Lyα forest structure. As we saw in the case of pressure, resolving small-scale structure is not only required to correctly predict the small-scale power, but also to predict the large-scale power (i.e., recall the factor of 1.1 increase, caused by pressure, in the large-scale power across the line of sight in Figure 5). This is analogous to the need to correctly simulate the formation of individual galaxies before galaxy bias can be predicted. I investigate the resolution effects by running matched sets of simulations with identical box sizes but differing numbers of particles. The initial mode amplitudes in the different resolution simulations are identical up to the Nyquist frequency of each grid.

In Figure 6(a) I compare the power for $N = 128^3$ (*solid line*), or $N = 64^3$ (*dotted line*) to the power for $N = 256^3$, using a box size 4.44 $h^{-1}\,\mathrm{Mpc}$. The quantity plotted in the figure is $\delta P/P \equiv (P_N - P_{256})/P_{256}$. The 256^3 and 128^3 simulations agree very well [better than 5% for $k < 10\,(\,h^{-1}\,\mathrm{Mpc})^{-1}$] but the 64^3 box shows larger disagreement. (Note that the effect of insufficient resolution is qualitatively similar to the effect of pressure seen in Figure 5, and that the required resolution for convergence is roughly the scale of the smoothing by pressure.) I conclude that, for a mean particle spacing of $\sim 35\,h^{-1}\,\mathrm{kpc}$, the Ly$\alpha$ forest structure is effectively resolved, and that a factor of 2 or so worse resolution can be used if a high level of accuracy is not required, or if the sensitivity of the measurement is carefully restricted to large scales. I test this conclusion further in Figure 6(b), where I use an 8.89 $h^{-1}\,\mathrm{Mpc}$ box. The results are similar, but we see that decreasing the resolution quickly becomes quite harmful. These results are not improved if I compare simulations at fixed optical depth normalization (τ_0) instead of fixed $\bar{F}$.

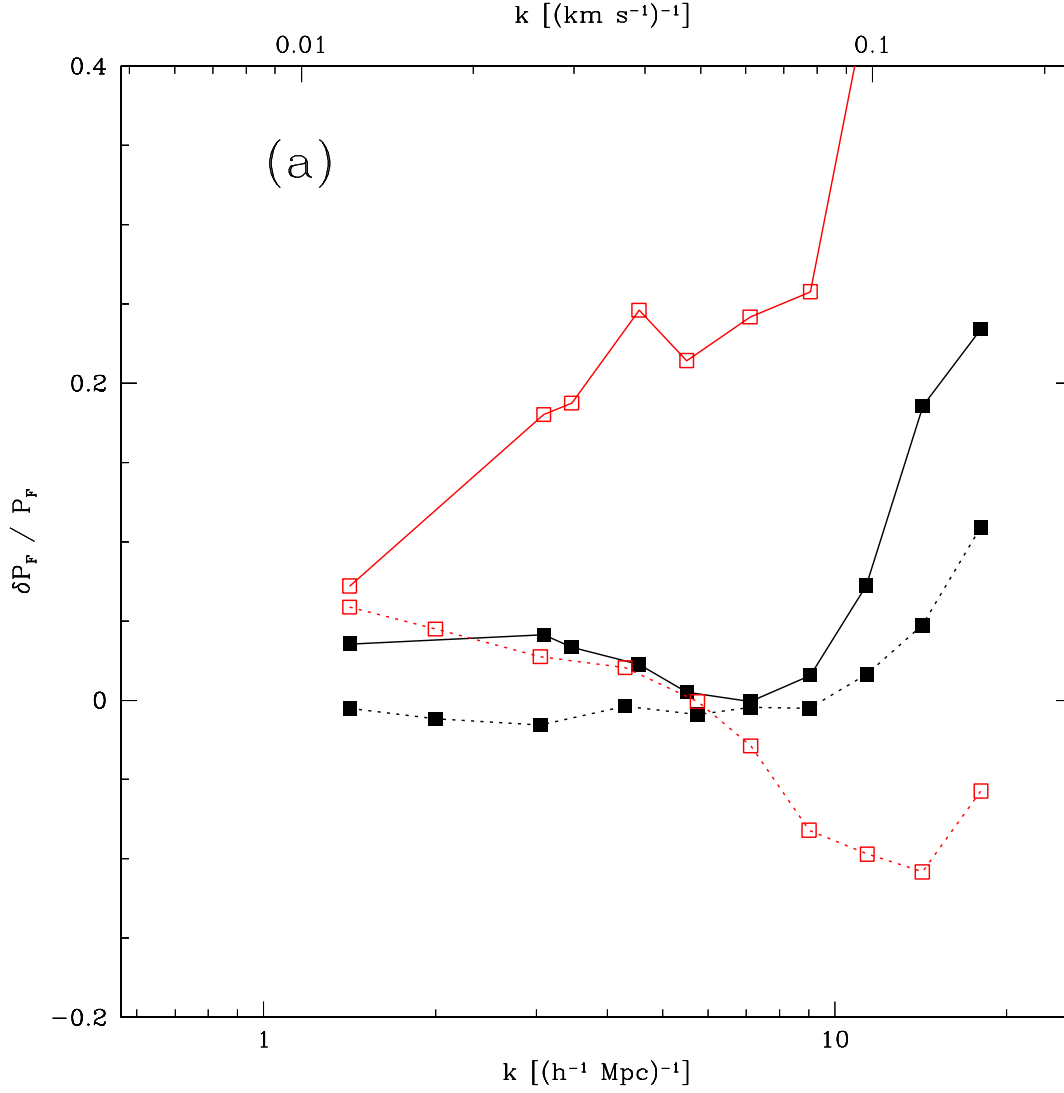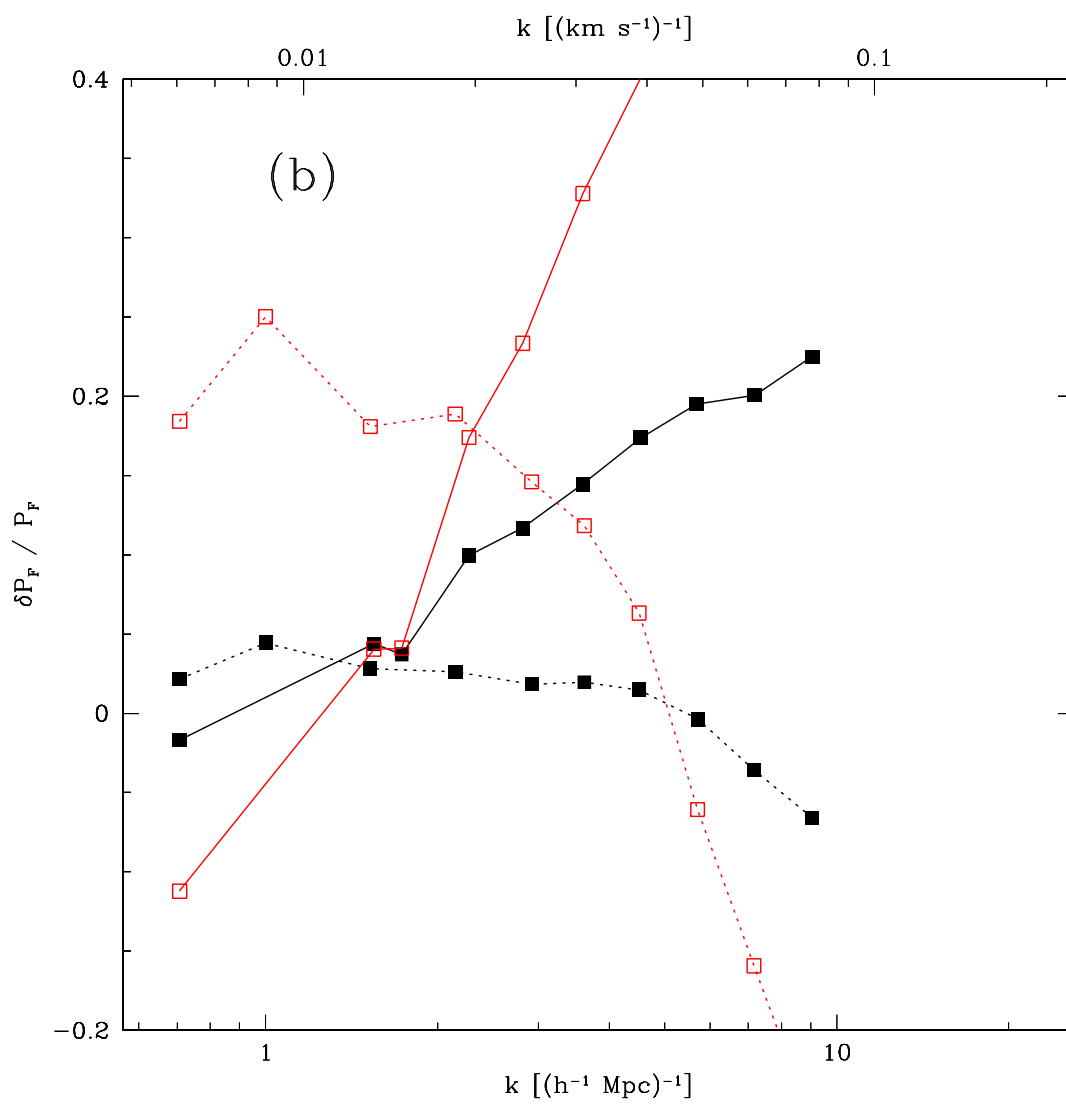Fig. 6.— Resolution test in an $L = 4.44\,h^{-1}$ Mpc box (a) and an $L = 8.89\,h^{-1}$ Mpc box (b). Black lines highlighted by filled squares show the ratio (minus 1) of power for $N = 128^3$ particles to power for $N = 256^3$ particles, along (*solid line*, $0.75 < \mu < 1.0$), and across (*dotted line*, $0.0 < \mu < 0.25$) the line of sight. Red lines with open squares show the ratio of $N = 64^3$ to $N = 256^3$.

In addition to obviously limiting the scale on which predictions can be made, the limited size of the simulation boxes can also influence the power spectrum results on all scales, because of the non-linear coupling of modes during gravitational evolution. In Figure 7 I compare 80, 40, and 20 h^{-1} Mpc boxes, with 512^3, 256^3 and 128^3 particles, respectively (it is not convenient to plot ratios because the k-modes are not identically spaced for different sized boxes). Power along (solid lines) and across (dotted lines) the line of sight refers to $0.75 < \mu < 1.0$ and $0.0 < \mu < 0.25$, as usual. For the lowest k modes in the box, it is difficult to see the precise level of agreement, because of statistical errors and discreteness in the values of $\mathbf{k}$ represented. I return to the issue of large scale convergence in the next subsection, where my computations of the linear theory bias are much less sensitive to statistical uncertainty. At higher k there is a systematic decrease in power as the box size is increased (the error for a 10 h^{-1} Mpc box is even larger than those shown). This is not surprising because the mass fluctuations are not perfectly linear even on the scale of the 40 h^{-1} Mpc box (see Figure 4). Fortunately, the difference between the 80 and 40 h^{-1} Mpc boxes is small enough that we can consider the 40 h^{-1} Mpc box to be sufficiently large.

My conclusion in this subsection is that 40 h^{-1} Mpc simulations with $\sim 1024^3$ particles should be sufficient to *completely simulate the Lyα forest flux power spectrum*, to $\sim 5\%$ accuracy; however, simulations of this size are beyond the scope of this work. In the rest of the paper, I solve the problem of competing demands for large box size and high resolution by splicing together the power spectra from pairs of large and small box simulations, using $L = 40\,h^{-1}$ Mpc for the large-scale power, and $L = 10\,h^{-1}$ Mpc for the small-scale power, both with $N = 256^3$.

In words (equations will come later), I correct for the poor resolution of the $L = 40\,h^{-1}$ Mpc, $N = 256^3$ boxes by comparing $L = 10\,h^{-1}$ Mpc, $N = 64^3$ simulations, which have the same resolution, to $L = 10\,h^{-1}$ Mpc, $N = 256^3$ simulations, which have sufficient resolution. For $k > 2\pi/(10\,h^{-1}$ Mpc) (the minimum k present in an $L = 10\,h^{-1}$ Mpc box), I can correct the power at a given k in the $L = 40\,h^{-1}$ Mpc simulation by the ratio, at the same k, of the power in the $L = 10\,h^{-1}$ Mpc, $N = 256^3$ simulations to the power in the $L = 10\,h^{-1}$ Mpc, $N = 64^3$ simulations. For larger scales, $k < 2\pi/(10\,h^{-1}$ Mpc), I assume (to be checked below) that I can use the $k = 2\pi/(10\,h^{-1}$ Mpc) correction factor, i.e., that the correction factor is independent of k. For small scales, $k \gtrsim 64\,\pi/(40\,h^{-1}$ Mpc) (one fourth of the Nyquist wavenumber of the large box) the resolution correction ceases to be a small factor (see Fig. 6), so at this k I switch from using the (corrected) power from the $L = 40\,h^{-1}$ Mpc box to using the power from the $L = 10\,h^{-1}$ Mpc, $N = 256^3$ simulation. I correct for the limited box size by a k-independent factor which is the ratio, at the splice point $k = 64\,\pi/(40\,h^{-1}$ Mpc), of the power in the $L = 40\,h^{-1}$ Mpc, $N = 256^3$ simulations to the power in $L = 10\,h^{-1}$ Mpc, $N = 64^3$ simulations.

In equations, the method just described for computing the corrected power, $P'_F(\mathbf{k})$, is the following: For $k_{\mathrm{min},10} < k < k_{\mathrm{Nyq},40}/4$ [where $k_{\mathrm{min},10} = 2\pi/(10\,h^{-1}$ Mpc) and $k_{\mathrm{Nyq},40} = 256\,\pi/(40\,h^{-1}$ Mpc)], I use the formula

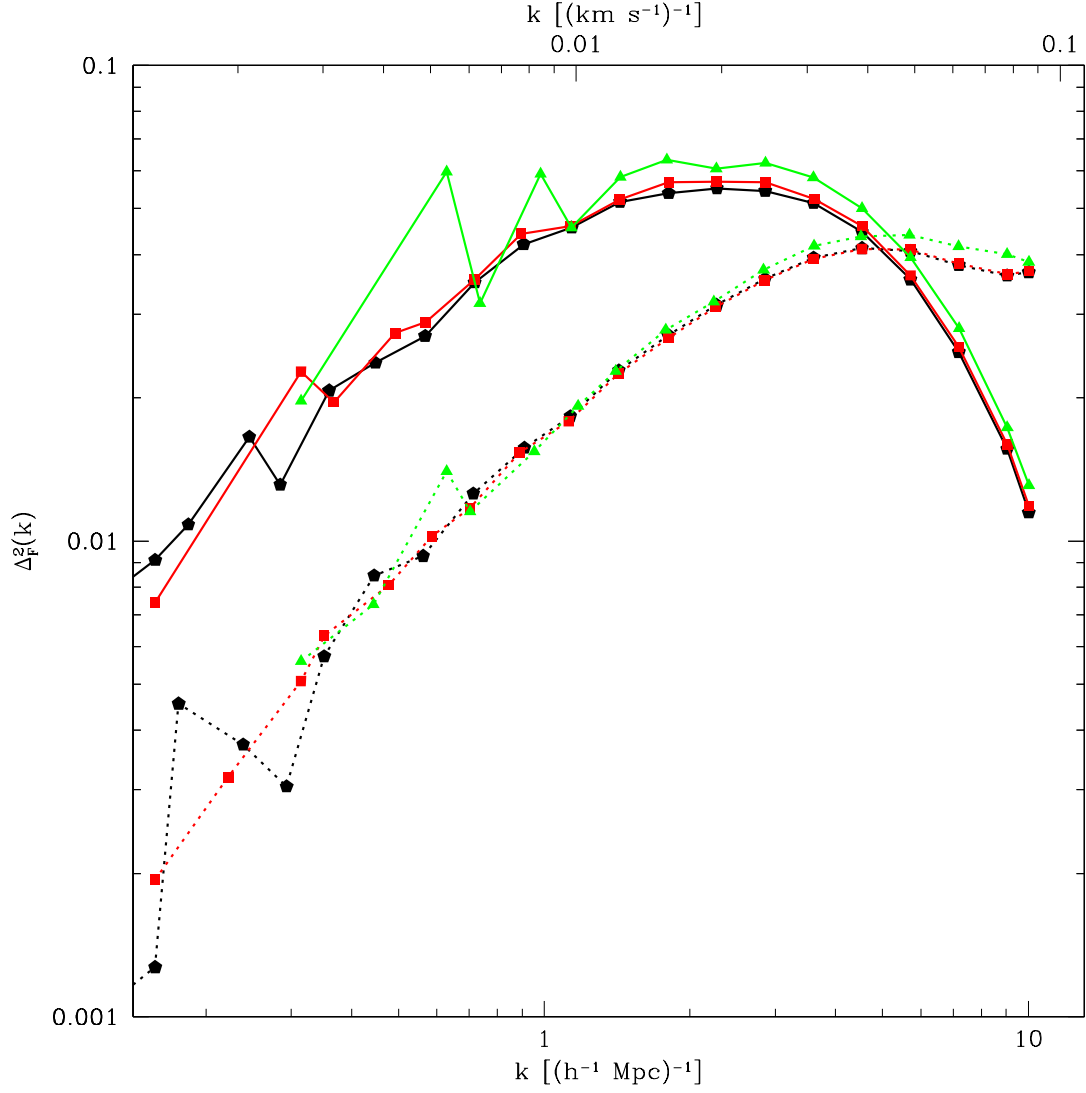$$P'_F(\mathbf{k}) \equiv P_{F,40,256}(\mathbf{k}) \frac{P_{F,10,256}(\mathbf{k})}{P_{F,10,64}(\mathbf{k})} \ , \tag{12}$$

Fig. 7.— Box size test. Black, red, and green lines (highlighted by *pentagons*, *squares*, and *triangles*) show the power in $L = 80$, 40, and 20 h^{-1} Mpc boxes, with $N = 512^3$, 256^3, and 128^3 particles, respectively (i.e., identical resolution). Power along (across) the line of sight is indicated by *solid* (*dotted*) lines.

where $P_{F,L,N^{1/3}}(\mathbf{k})$ is the flux power in simulations with box size L and number of particles N. For $k < k_{\mathrm{min},10}$, I use

$$P_F'(\mathbf{k}) \equiv P_{F,40,256}(\mathbf{k}) \frac{P_{F,10,256}(k_{\mathrm{min},10},\mu)}{P_{F,10,64}(k_{\mathrm{min},10},\mu)} \ , \tag{13}$$

and for $k > k_{\mathrm{Nyq},40}/4$ I use

$$P_F'(\mathbf{k}) \equiv P_{F,10,256}(\mathbf{k}) \frac{P_{F,40,256}(k_{\mathrm{Nyq},40}/4,\mu)}{P_{F,10,64}(k_{\mathrm{Nyq},40}/4,\mu)} \ . \tag{14}$$

In practice, these correction factors are interpolated between bins in k and μ (because the $\mathbf{k}$ spacing is different in simulations with different L). Ultimately, more exact results will be obtained by running larger simulations, but, judging from the preceding tests, this procedure should give reasonably accurate results.

Figure 8 shows a test of the convergence of the full correction procedure. Normally I use $L = 40\,h^{-1}\,\mathrm{Mpc}$ and $L = 10\,h^{-1}\,\mathrm{Mpc}$ boxes with $N = 256^3$, and assess the effect of limited box size and resolution by comparison with $L = 10\,h^{-1}\,\mathrm{Mpc}$, $N = 64^3$ (the result of this standard method is shown as red lines highlighted by triangles), but in this figure I also show the results of applying the same correction procedure using an $L = 80\,h^{-1}\,\mathrm{Mpc}$ and an $L = 20\,h^{-1}\,\mathrm{Mpc}$ box, both with $N = 512^3$, and an $L = 20\,h^{-1}\,\mathrm{Mpc}$ box with $N = 128^3$ (black lines and squares). This tests the assumption that the resolution correction can be extrapolated to large scales, even though it is estimated using an insufficiently large $10\,h^{-1}\,\mathrm{Mpc}$ box, and that the rather large box size correction that is needed ($\sim 30\%$ along the line of sight) is reasonably accurate. The results are generally good, with agreement to almost 10% in the power for $0.5\,(h^{-1}\,\mathrm{Mpc})^{-1} < k < 10\,(h^{-1}\,\mathrm{Mpc})^{-1}$ [for $k < 0.5\,(h^{-1}\,\mathrm{Mpc})^{-1}$, statistical errors obscure the comparison].

3.4. Lyα Forest Bias

The preceding calculations give a method for computing the Lyα forest flux power on scales smaller than $\sim 40\,h^{-1}\,\mathrm{Mpc}$ (although many simulations would be required in order to reduce the statistical error for the lowest k modes). This is sufficient for past one-dimensional power spectrum measurements, which probed scales less than $\sim 20\,h^{-1}\,\mathrm{Mpc}$ (Croft et al. 1999, 2000; McDonald et al. 2000), but upcoming SDSS one-dimensional results will reach $\sim 80\,h^{-1}\,\mathrm{Mpc}$ (limited by uncertainties in the quasar continuum; L. Hui, private communication), and measurements using multiple lines of sight may go even farther. In order to extend the calculations of the Lyα forest power to larger scales than we can conveniently reach directly through simulations, it is useful to revert to the "linear theory with bias" picture that is usually used to describe large-scale clustering of galaxies (e.g., Blanton et al. 2000; Benson et al. 2000; Cen & Ostriker 2000; Somerville et al. 2001). Within this picture we may also gain a deeper understanding of the $\mathbf{k}$ dependence of the flux power spectrum that we see in Figure 8.

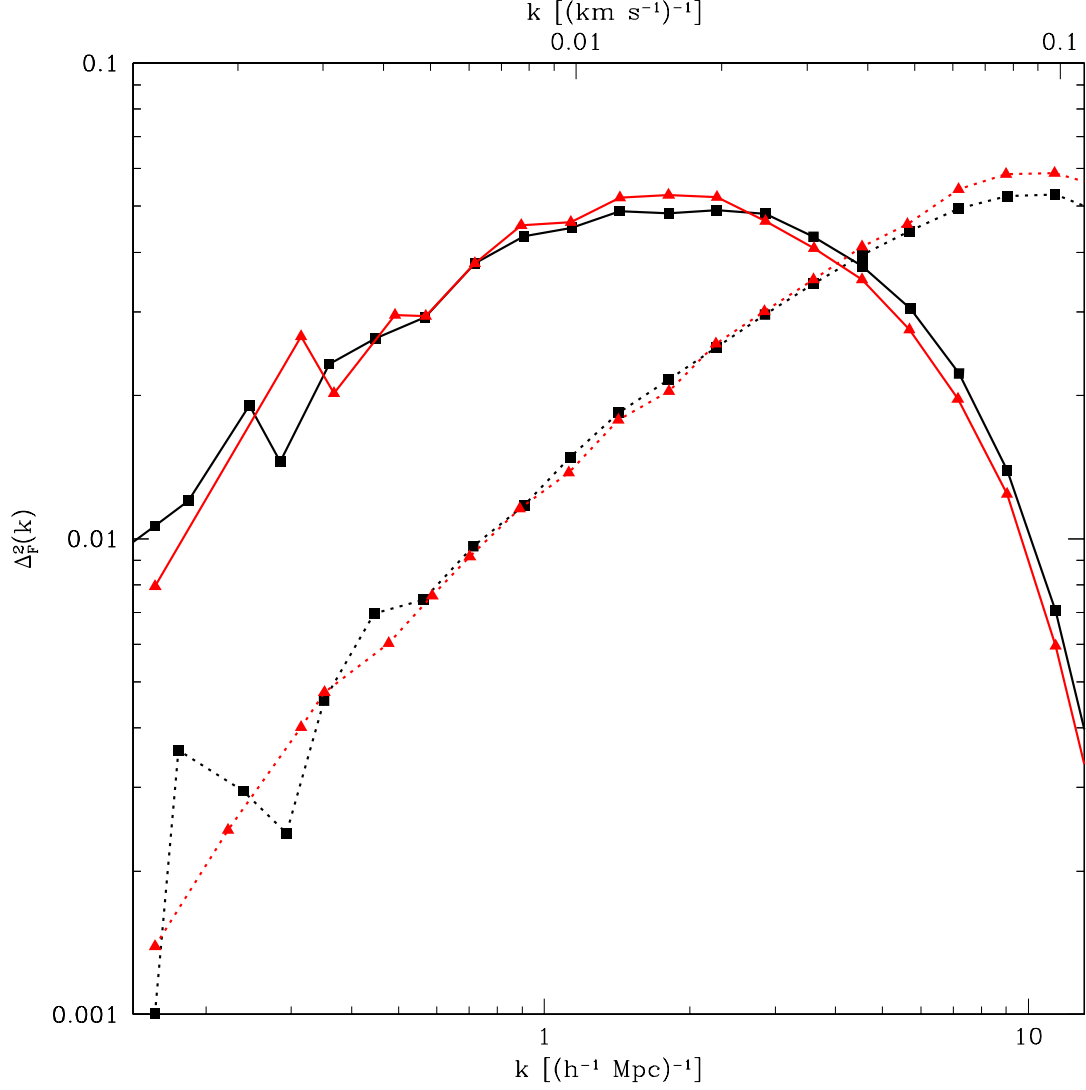We seek to determine the relationship between fluctuations in the mass density field smoothed

Fig. 8.— Test of the corrections for box size and resolution. Solid lines show power along the line of sight, dotted lines across the line of sight. Red lines (highlighted by triangles) show the results of our standard combination of $L = 40\,h^{-1}\,\mathrm{Mpc}$ and $L = 10\,h^{-1}\,\mathrm{Mpc}$ boxes with $N = 256^3$. Black lines (squares) show the combination of an $L = 80\,h^{-1}\,\mathrm{Mpc}$ and a $L = 20\,h^{-1}\,\mathrm{Mpc}$ box, with $N = 512^3$.

in three-dimensions on some large scale, δ_s, and fluctuations in the Lyα forest transmitted flux field similarly smoothed, F_s. Furthermore, in contrast to the case of galaxies, the non-linear transformation applied to the Lyα forest field after the transformation into redshift space [i.e., $\exp(-\tau)$] means that for the Lyα forest the relationship between the large-scale flux fluctuations and the gradient of peculiar velocity along the line of sight, smoothed on the same scale, must be determined separately from the $F_s - \delta_s$ relation. I define $\eta \equiv -H^{-1}dv_\parallel/dr_\parallel$, where $v_\parallel$ is the peculiar velocity along the line of sight, and $r_\parallel$ is the distance along the line of sight, so η_s is the smoothed gradient of the line of sight velocity. Two bias parameters are needed: one, which I will call b_δ, that relates large-scale mass density fluctuations to transmitted flux fluctuations, and one, b_η, that relates fluctuations in the gradient of the peculiar velocity field along the line of sight to flux fluctuations.

The general formalism for bias calculations is discussed extensively in Dekel & Lahav (1998), and Appendix C of McDonald et al. (2000) discussed its application to the Lyα forest. The linear theory, redshift-space flux power spectrum, $P_{F,L}(k, \mu)$, is related to the real-space mass power, $P_L(k)$, by the familiar (Kaiser 1987) formula:

$$P_{F,L}(k, \mu) = b_\delta^2 \ (1 + \beta\mu^2)^2 P_L(k) \ , \tag{15}$$

where $\beta = \Omega^{0.6}(z) \ b_\eta/b_\delta$. For $\Omega_m = 0.4$ and $\Omega_\Lambda = 0.6$, $\Omega^{0.6}(z = 2.25) = 0.975$, so the result is very insensitive to cosmology. As discussed in McDonald et al. (2000), the two bias parameters come essentially from a Taylor series expansion of F_s, i.e., $F_s(\delta_s, \eta_s)/F_s(\delta_s = \eta_s = 0) \simeq 1 + b_\delta \ \delta_s + b_\eta \ \eta_s$, with

$$b_\delta = \left. \frac{1}{F_s} \frac{dF_s}{d\delta_s} \right|_{\eta_s=0} \ , \tag{16}$$

and

$$b_\eta = \left. \frac{1}{F_s} \frac{dF_s}{d\eta_s} \right|_{\delta_s=0} \ . \tag{17}$$

It is these derivatives that we must measure from our simulations.

An obvious way to proceed would be to define F_s, δ_s, and η_s by, for example, applying a Gaussian or top-hat smoothing kernel to the same simulation boxes discussed in §3.3. However, if I took this approach the simulation boxes would have to be even larger than the size required for convergence of the small scale structure (see Figure 7), because they would have to be large enough to contain multiple internal volumes that were separately large enough to be in the linear regime. Given that the simultaneous requirements on box size and resolution already overburden my computing capabilities, I use a novel technique to compute the derivatives. I take advantage of the fact that small-scale structure in a sufficiently large, spherical, over-dense or under-dense region evolves identically to structure in a whole universe with the same density. I can therefore use my numerical simulations to simulate the evolution of structure in a large-scale perturbation by simply modifying the cosmological parameters that are input so they represent the perturbation instead of the background universe. Using this trick, I can compute F_s from δ_s and η_s using the largest averaging volume that I can possibly simulate: one full simulation cube. Using multiple cubes with

different values of the perturbation parameters, δ_s and η_s (I use $\delta_s = \pm 0.1$ and $\eta_s = \pm 0.1$), I can compute the derivatives in equations (16 and 17) numerically. Note that, if I have truly reached the scale where linear theory holds, the size of the smoothing volume should not matter, since b_δ and b_η are in theory independent of scale.

I am going to assume that the growth of small-scale structure in a region is determined entirely by the large-scale density (as opposed to the complete large-scale deformation tensor). This is not strictly true, but it greatly simplifies the calculations. In order to check this assumption, it is necessary to run simulations with anisotropic expansion.

Varying δ_s for a simulation cube still requires re-running the simulation, to correctly account for the dynamical effect of changes in the mean density on the growth of small scale structure. In practice this means that, using the same set of initial particle positions and velocities, I evolve the simulation forward to expansion factor $a' = a(1 - 1/3\,\delta_s)$, where a is the original expansion factor, and use matter density parameter $\Omega'_m = (1 + 5/3\,\delta_s)$, where originally $\Omega_m \simeq 1$ (I correctly account for the presence of the cosmological constant and deviation of Ω_m from 1, but this is irrelevant in practice at $z > 2$). F_s is simply the mean flux averaged over the entire modified box. The value of F_s changes relative to the original simulation, not only because of the change in overall mean baryon density, but also because of the change in the small-scale distributions of densities and peculiar velocities.

Since I am ignoring the possibility that the anisotropic expansion of a large-scale region is important to the growth of small-scale structure within it, varying η_s (at fixed δ_s) within a simulation cube, for the purpose of constructing Lyα forest spectra, is basically trivial. All optical depths are divided by a factor $(1 - \eta_s)$, and the width of the thermal broadening kernel (i.e., $T^{1/2}$), measured in mesh cells, is divided by the same factor (bulk velocities measured in mesh cells are unchanged because the overall density parameter, i.e., Ω within the perturbation, is unchanged). This procedure is equivalent to using $(1 - \eta_s)H(z)$ in place of $H(z)$ when creating spectra.

Applying these transformations to a set of eight $L = 40\,h^{-1}\,\mathrm{Mpc}$, $N = 256^3$ simulations, I find $b_\delta = -0.1511 \pm 0.0006$ and $b_\eta = -0.1722 \pm 0.0005$, or, in terms of parameters whose relevance to the AP test is clearer, $b_\delta^2 = 0.0228 \pm 0.0002$, and $\beta = 1.112 \pm 0.005$. Good statistical precision can be achieved using relatively few simulations because the parameters are being computed as differences between simulations with identical initial conditions. To check the convergence with box size, I run $L = 20\,h^{-1}\,\mathrm{Mpc}$, $N = 128^3$ simulations, finding $b_\delta^2 = 0.0259 \pm 0.0005$, and $\beta = 1.052 \pm 0.013$. The 6% error in β (equivalent to 7% error in the ratio of power along to across the line of sight) is acceptable for the present purpose. The 14% error in b_δ^2, which leads to an isotropic error on $P_F(\mathbf{k})$, would be disturbing if my purpose was to measure the amplitude of the primordial density fluctuations, but is not a problem for the AP test. Finally, I test the convergence using an $L = 80\,h^{-1}\,\mathrm{Mpc}$, $N = 512^3$ simulation, finding agreement with $L = 40\,h^{-1}\,\mathrm{Mpc}$ to better than 1% for both b_δ^2 and β.

I correct the bias parameters for the limited resolution of the $L = 40\,h^{-1}\,\mathrm{Mpc}$ simulations by applying the same corrections that are used for the power spectrum in the lowest k bins, i.e., by

solving the following two equations for b'^2_δ and β':

$$b'^2_\delta = b^2_\delta \frac{P_{F,10,256}(k_{\min,10}, \mu = 0)}{P_{F,10,64}(k_{\min,10}, \mu = 0)} \ , \tag{18}$$

and

$$b'^2_\delta (1 + \beta')^2 = b^2_\delta (1 + \beta)^2 \frac{P_{F,10,256}(k_{\min,10}, \mu = 1)}{P_{F,10,64}(k_{\min,10}, \mu = 1)} \ . \tag{19}$$

The result is $b'^2_\delta = 0.0173 \pm 0.0003$ and $\beta' = 1.580 \pm 0.022$. I check these bias correction factors by recomputing them using $L = 20\,h^{-1}\,\mathrm{Mpc}$, $N = 512^3$ box and a similar sized 128^3 box, and find that the correction to β changes by only 1%, while the correction to b^2_δ changes by only 4%, indicating that my results on the largest scales have converged.

In conclusion, I have achieved something remarkable: a direct calculation of the linear theory bias parameters of the Lyα forest, which can be used to extend the results of numerical simulations for comparison with data on arbitrarily large scales (although the importance of anisotropic large-scale expansion remains to be investigated). I demonstrated that my calculations have truly reached the linear regime, i.e., the bias parameters don't change with increasing scale. The results of this subsection and §3.3 suggest that combinations of $L = 40\,h^{-1}\,\mathrm{Mpc}$, $N = 512^3$ simulations with smaller box size simulations ($L \sim 20\,h^{-1}\,\mathrm{Mpc}$) to compute resolution corrections should be sufficient to compute the Lyα forest power spectrum for all $\mathbf{k}$, to much better than 10% (as demonstrated in Figure 8, my method is limited to $\sim 10\%$ accuracy using 256^3 simulations because the largest fully resolved simulation I can run is only $L \simeq 10\,h^{-1}\,\mathrm{Mpc}$). With the addition of fully hydrodynamic simulations to compute corrections to the HPM approximation, we should be fully prepared to interpret the clustering in large future data sets.

3.5. Analytic Formula for $P_F(\mathbf{k})$

Equation 15 provides a convenient analytic description of the power spectrum at very small k, but it is useful to have an analytic formula that can describe the power for all $\mathbf{k}$. Since no such formula has been successfully derived even in the simpler case of the dark matter power spectrum, I follow the usual strategy of fitting a parameterized formula to the simulation results. The three-dimensional real-space power spectrum of the dark matter, in CDM models, and on the scale of the Lyα forest, increases above the linear prediction with increasing k (e.g., Ma 1998), so we might guess that the Lyα forest flux power will behave similarly, although there is no guarantee that it will. Non-linear peculiar velocities should suppress the power along the line of sight [the "fingers of god" effect, see Jing & Boerner (2000) for the state of the art]. In the Lyα forest, the addition of pressure and thermal broadening will further modify the high-k power.

Fortunately, my simulations show that the complicated transformation to Lyα forest transmitted flux preserves qualitatively the features expected for dark matter, so it is easy to guess a

working fitting formula. I use the following general form:

$$P_F(k, \mu) = b_\delta^2 (1 + \beta \mu^2)^2 P_L(k) \, D(k, \mu) \,, \tag{20}$$

where

$$D(k, \mu) \equiv \exp \left\{ \left[\frac{k}{k_{NL}} \right]^{\alpha_{NL}} - \left[\frac{k}{k_P} \right]^{\alpha_P} - \left[\frac{k_\parallel}{k_V(k)} \right]^{\alpha_V} \right\} \,, \tag{21}$$

and $k_V(k) = k_{V0} \, (1 + k/k_V')^{\alpha_V'}$. The first term in the exponential allows for the isotropic increase in power due to non-linear growth, the second term for the isotropic suppression by pressure, and the third for the suppression by non-linear peculiar velocities and temperature along the line of sight. [The dependence of k_V on k is motivated by the finding of Jing & Boerner (2000) that the smoothing kernel associated with non-linear peculiar velocities cannot be written as a simple function of $k_\parallel = \mu k$ alone. I also find this result for the Lyα forest.]

As an example, I fit equation (20) to the results of my standard $P_F(\mathbf{k})$ computation, using the values of $b_\delta^2 = 0.0173$ and $\beta = 1.58$ obtained by the procedure described in §3.4. The error bars I use for the fit are obtained by computing the dispersion between the power spectrum results from eight simulations with different random initial conditions. To prevent the highest k points from completely dominating the fit, I have set a minimum size for the error bars of 5%. The fit is very good, better than 5% or the statistical errors, in the sense that $\chi^2/\nu = 0.8$. The fitted parameters are: $k_{NL} = 6.77 \ (h^{-1} \, \mathrm{Mpc})^{-1}$, $\alpha_{NL} = 0.550$, $k_P = 15.9 \ (h^{-1} \, \mathrm{Mpc})^{-1}$, $\alpha_P = 2.12$, $k_{V0} = 0.819 \ (h^{-1} \, \mathrm{Mpc})^{-1}$, $\alpha_V = 1.50$, $k_V' = 0.917 \ (h^{-1} \, \mathrm{Mpc})^{-1}$, and $\alpha_V' = 0.528$. Figure 9(a) shows the results of the fit with the initial real space power spectrum divided out, i.e., $P_F(\mathbf{k})/P_L(k)$, and Figure 9(b) shows just the small-scale kernel, $D(k, \mu) = P_F(\mathbf{k})/ \left[b_\delta^2 \left(1 + \beta \mu^2 \right)^2 P_L(k) \right]$. These figures summarize the primary result of this section — I have established a procedure for computing the Lyα forest power spectrum for all $\mathbf{k}$ from HPM simulations, with reasonably well understood, if not completely eliminated, numerical errors.

In the next section I will simply repeat the procedures described in this section for different values of the cosmological and Lyα forest model parameters. I will use the fitting formula presented here as a convenient way to present the results of many different models without giving large tables of binned power spectrum results. In all cases I find good agreement ($\chi^2/\nu < 1$) between the power spectrum points and the best fit. Note that I have no way to compute the parameters of the fitting formula from the model parameters, other than running the necessary simulations and doing the fit, so the formula is only useful for interpolating between models, not for extrapolating to models outside the basic parameter space in which I provide results. Equation (20) also eliminates the problem of interpolating between many power spectrum points, binned in k and μ, when computing quantities which are integrals over the three-dimensional power spectrum, such as the correlation function or the one-dimensional power spectrum.
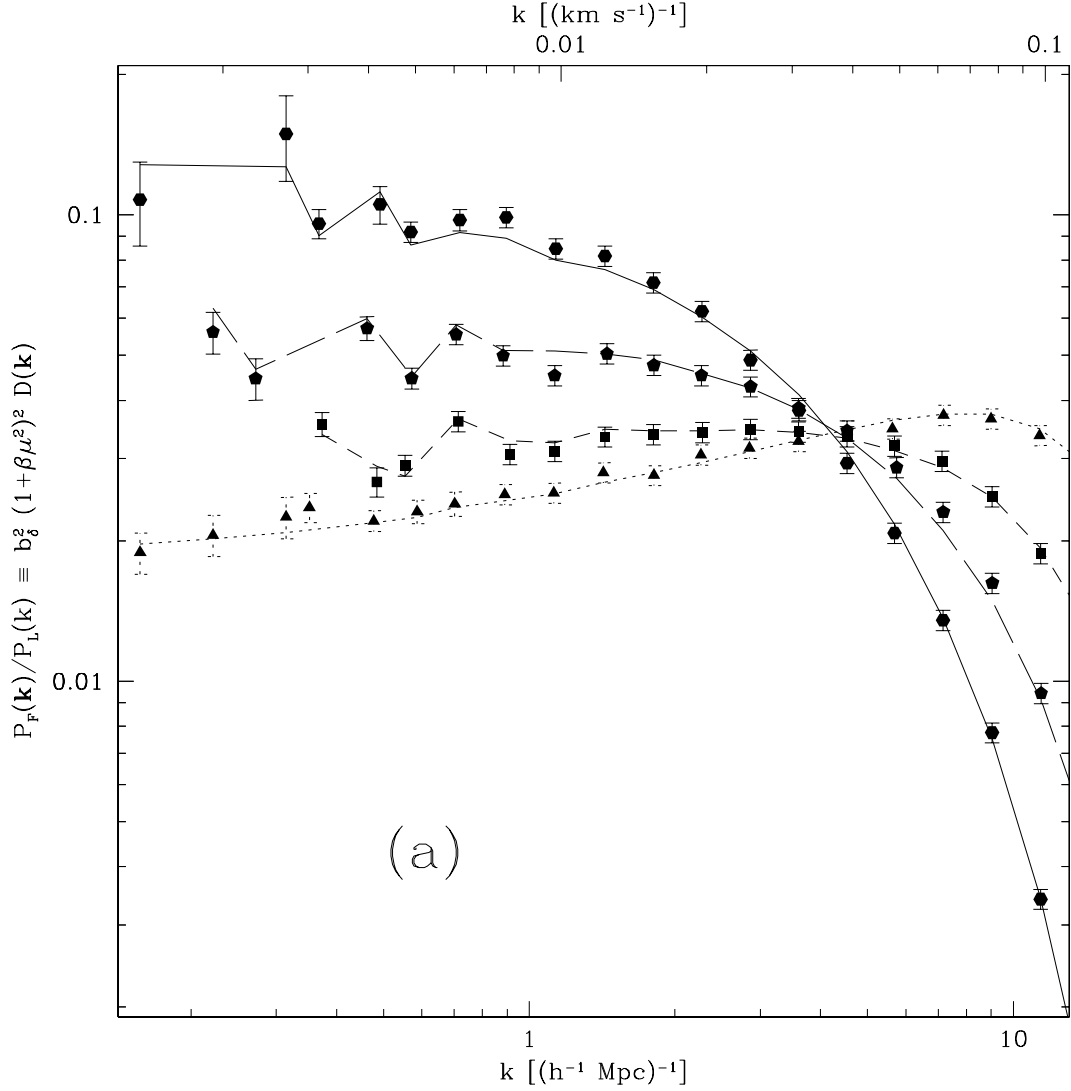
Fig. 9.— Results for the flux power spectrum. In (a), the *triangles, squares, pentagons, and hexagons* show, for μ bins 0-0.25, 0.25-0.5, 0.5-0.75, and 0.75-1.0, the ratio of the Lyα forest power to the linear theory (real space) mass power at the the same **k**. The lines show my analytic formula, using the computed values for b_δ^2 and β, with $D(\mathbf{k})$ fit to the simulation points. (b) is similar except $b_\delta^2(1 + \beta\mu^2)^2$ has been divided out, leaving only $D(k, \mu)$.
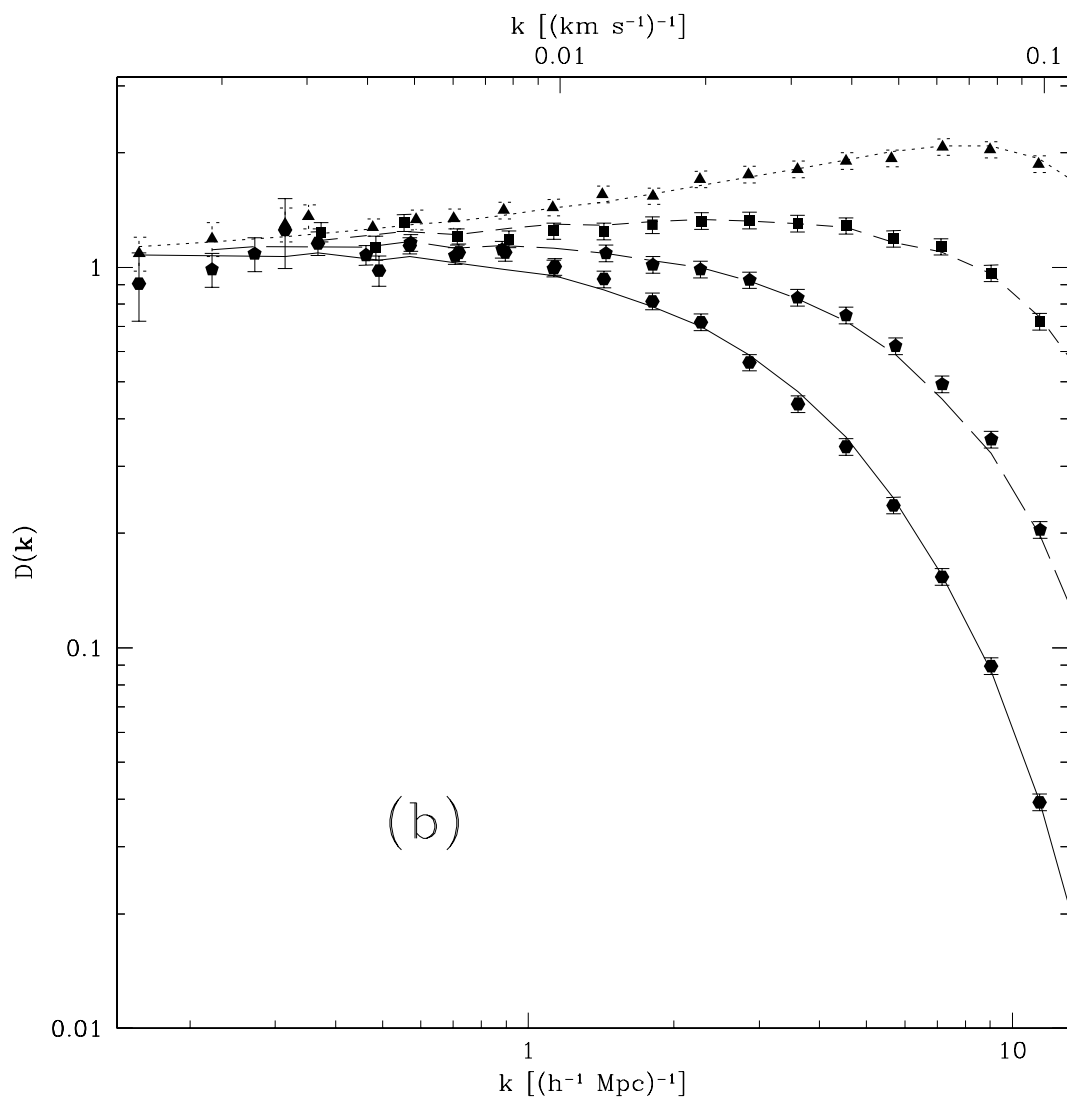
4. PARAMETER DEPENDENCE OF THE POWER SPECTRUM

In order to carry out a complete analysis of Lyα forest data, it will be necessary to perform the kind of multi-parameter, maximum-likelihood analysis that is commonly applied to the CMB power spectrum (e.g., Tegmark & Zaldarriaga 2000), involving a many-dimensional grid of Lyα forest model predictions (Zaldarriaga et al. 2000). Here I am content to compute the derivatives of $P_F(\mathbf{k})$ with respect to the parameters at a typical point in parameter-space. These derivatives show the basic trends, and allow me to perform Fisher matrix calculations of the expected parameter constraining power of future observations (see, for example, Eisenstein, Hu, & Tegmark 1999).

I choose to study a model in which the flux power spectrum depends on five free parameters: A_1, the value of $\Delta_L^2(k) \equiv k^3 P_L(k)/(2\pi^2)$ at $k_1 = 2\pi(h^{-1}\,\mathrm{Mpc})^{-1}$, n_1, the power law index of the power spectrum at k_1, $T_{1.4}$, $\gamma - 1$, and $\bar{F}$, which together form the parameter vector $\mathbf{p} = (\bar{F},\ T_{1.4},\ \gamma - 1,\ A_1,\ n_1)$. I use a CDM shape for the power spectrum, not a true power law, but for simplicity I do not allow the shape to change, other than by an overall tilt controlled by n_1. My results can be applied to any cosmological model in which the power spectrum can be approximated by the CDM shape, by computing A_1 and n_1 for the power spectrum of the model.

I vary each of the parameters and compute the flux power spectrum as described in §3. The central set of parameters is $\mathbf{p}_0 = (0.8,\ 20000,\ 0.5,\ 1.38,\ -2.58)$ (these values for A_1 and n_1 are equivalent to $\sigma_8 = 0.79$ and $n = 0.95$ for the flat, ΛCDM model, with $\Omega_m = 0.4$ and $h = 0.65$). In Figures 10(a,b,c) I plot the quantity

$$\frac{\delta P_F}{P_F}(\delta\mathbf{p}) \equiv \frac{P_F(\mathbf{p}_0 + \delta\mathbf{p}) - P_F(\mathbf{p}_0 - \delta\mathbf{p})}{P_F(\mathbf{p}_0)}\ , \tag{22}$$

where $\delta\mathbf{p}$ is some variation of the parameters. The values of $\delta\mathbf{p}$ I choose are intended to represent roughly the current level of uncertainty in each parameter.

When we look at $\delta P_F/P_F$ for different parameter variations, we will be particularly interested in any parameter variations that could lead to substantial variations in the ratio of the power along the line of sight to the power across the line of sight (i.e., variations in β for small k), because these could lead to degeneracy between the parameter being varied and the transverse scale factor $f(z)$ that is measured in the AP test. Fortunately, the one-dimensional power spectrum can be measured very accurately from single lines of sight and used to constrain the model parameters, so we only need to worry if there is model dependence of the power spectrum anisotropy for relatively small variations in the parameters.

In Figure 10(a), the black lines highlighted by filled squares show the variation in power spectrum amplitude, $\delta A_1/A_1 = 0.29/1.38 = 0.21$, with all of the other parameters fixed. We see the expected increase in large-scale power both along and across the line of sight, with the increase in flux power significantly less than proportional to the increase in initial mass power, as found by Croft et al. (1999; 2000), and McDonald et al. (2000). For $k \gtrsim 1 - 2(h^{-1}\,\mathrm{Mpc})^{-1}$, it is interesting to note that increasing the mass power actually decreases the flux power along the line of sight,
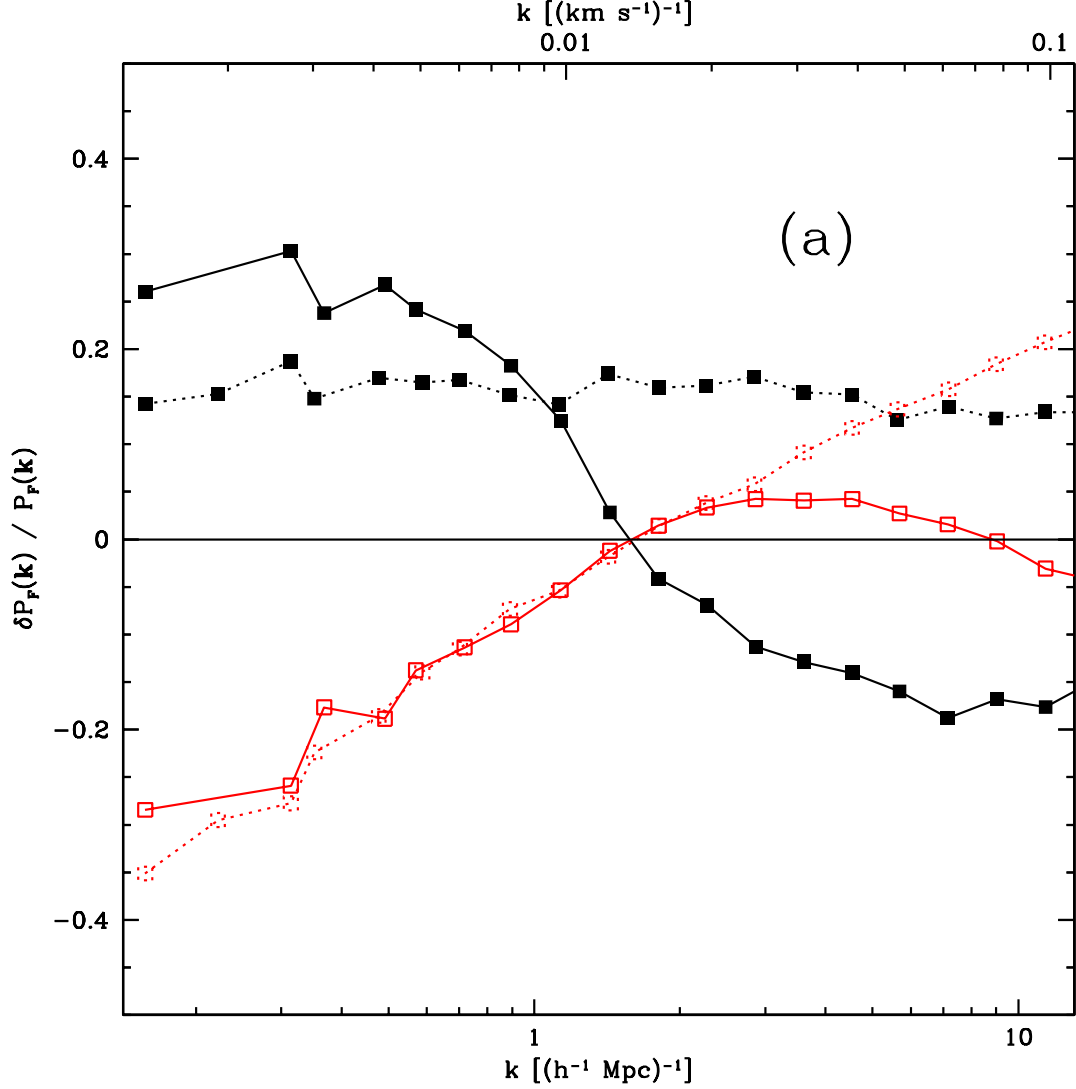
Fig. 10.— Fractional variation of $P_F(\mathbf{k})$ with variation of the model parameters. The *solid* lines are power along the line of sight, the *dotted* are transverse power. As discussed in the text, δP_F is the difference between results for a positive and negative variation of each parameter, i.e., $\delta P_F \equiv P_F(p + \delta p) - P_F(p - \delta p)$, where p is the parameter. In (a), *black lines* highlighted by *solid squares* show variation of A_1, by ± 0.29, and *red lines* (*open squares*) show variation of n_1, by ± 0.1. In (b), *black lines* (*solid squares*) show variation of $T_{1.4}$ by ± 2000 K, and *red lines* (*open squares*) show variation of $\gamma - 1$ by ± 0.1. In (c), *black lines* (*solid squares*) show variation of $\bar{F}$ by ± 0.025, and *red lines* (*open squares*) show variation of z by ± 0.25 (see text).
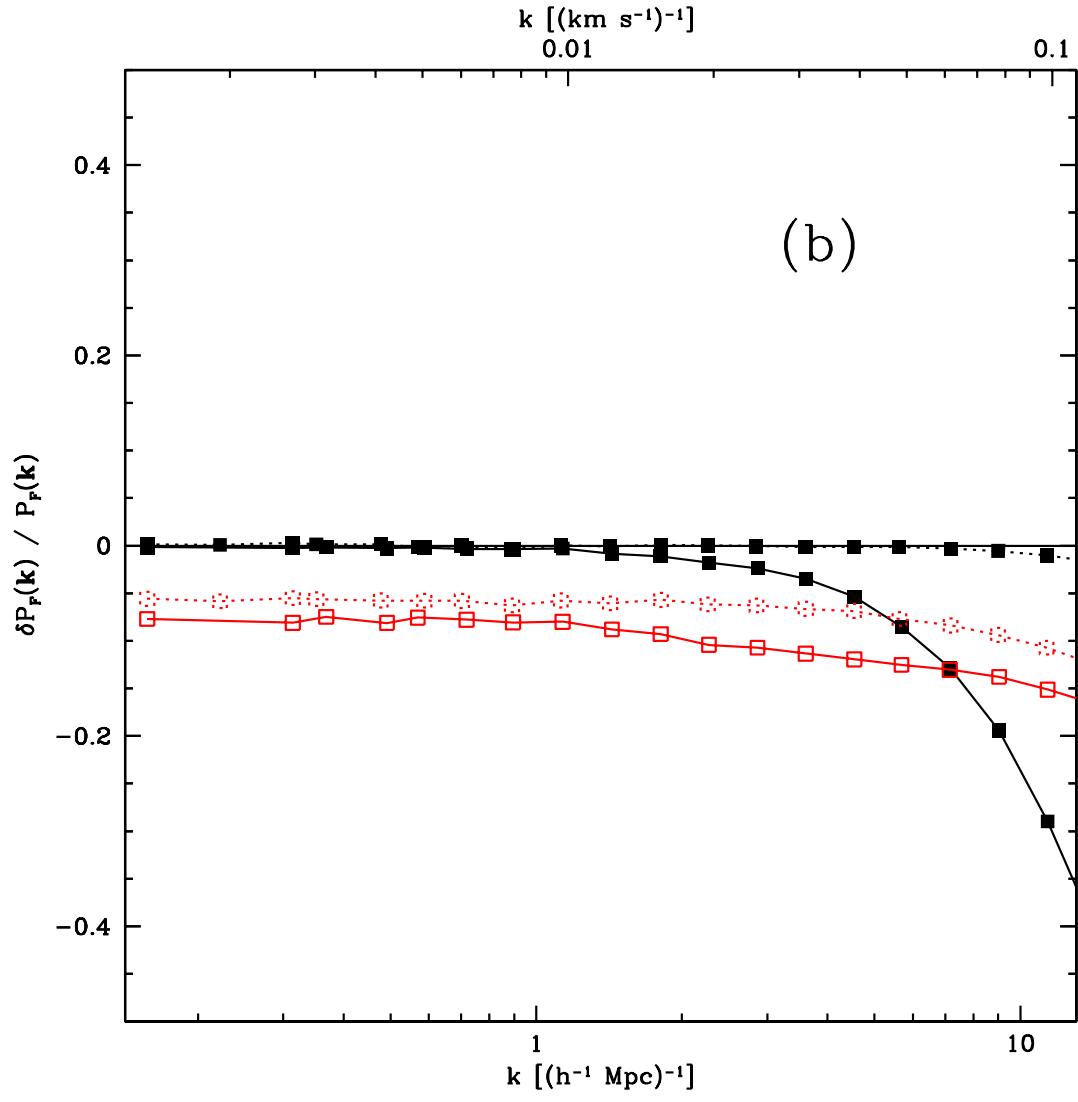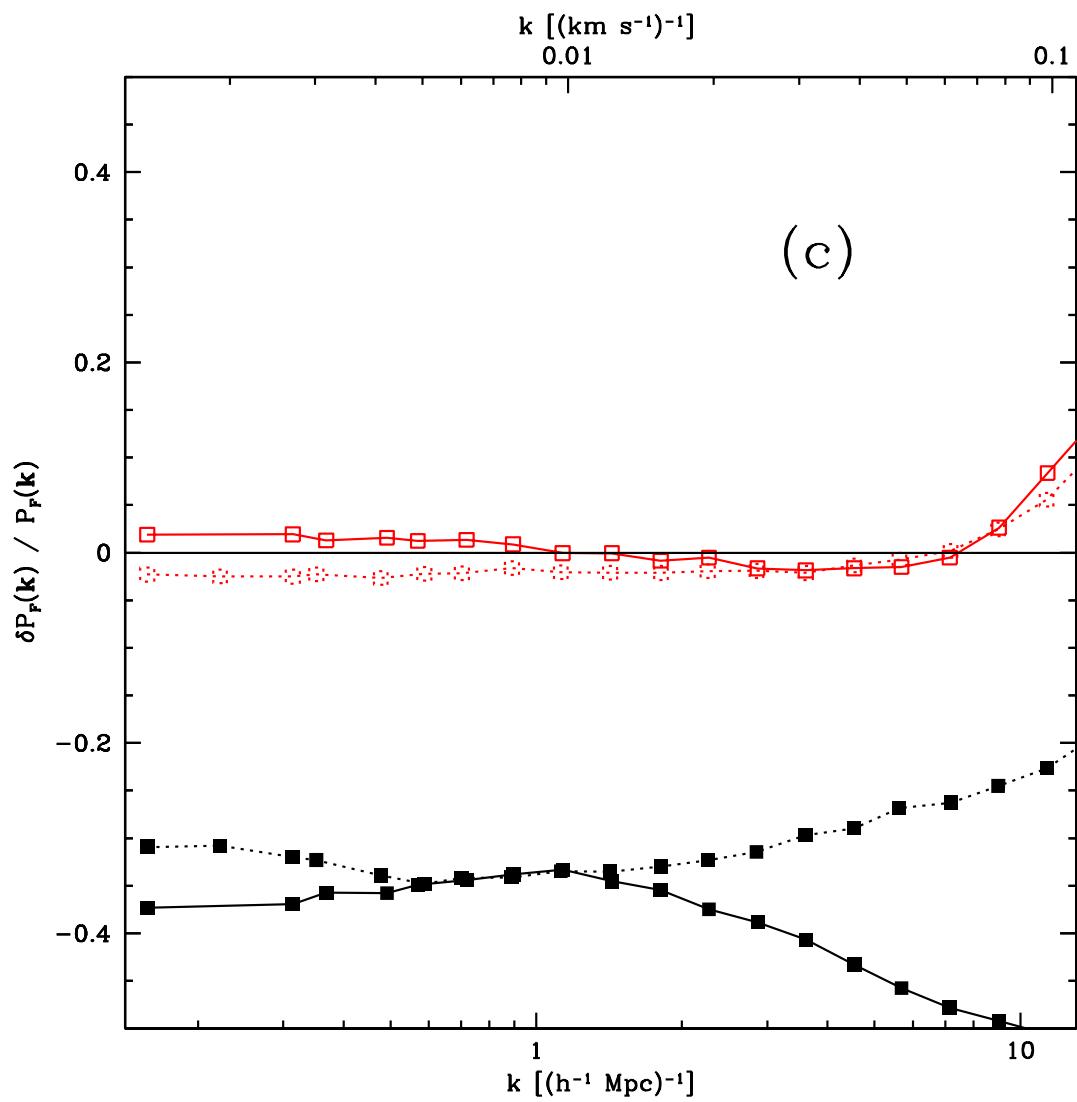
presumably by increasing the power suppression by non-linear peculiar velocities. The variation of $\sim \pm 5\%$ in the ratio of power along to across the line of sight on large scales, equivalent to a similar variation in β, is actually not a problem for the AP test because the measurements by McDonald et al. (2000) and Croft et al. (2000) already constrain the power spectrum amplitude to better than $\sim 20\%$. The variation in power spectrum anisotropy will become more of a problem for quasar pairs with separations less than a few arcminutes, where the power suppression by non-linear peculiar velocities is important.

The red lines, highlighted by open squares, in Figure 10(a) show the variation $\delta n_1 = 0.1$. (Due to imperfect planning, this variation is at fixed σ_1, not fixed A_1, where σ_1 is the rms fluctuation of the linear theory mass field in spheres with radius $1\, h^{-1}\,\mathrm{Mpc}$; however, the difference is not important to the qualitative presentation in the figure.) At low k, the effect of changing n_1 appears to be a straightforward, isotropic, change in the slope of the flux power spectrum. At high k, where increasing n_1 means increased initial power, $P_F(\mathbf{k})$ is again suppressed along the line of sight.

Figure 10(b) shows variations of the temperature-density relation, $\delta T_{1.4} = 2000$ K (black lines with solid squares) and $\delta(\gamma - 1) = 0.1$ (red lines with open squares) (actually, $\gamma - 1$ was only varied by ± 0.05 in the simulations so δP has been multiplied by 2). The variation with $T_{1.4}$ is just what might be expected from the corresponding change in thermal broadening. The thermal broadening suppresses the optical depth power by $\exp(-k^2 T)$, so, for $2\,\delta T = 4000$ K, the increased suppression is by $\exp(-k^2\, 4000\mathrm{K}) = \exp[-(k\, 5.75\,\mathrm{km\,s^{-1}})^2]$, or a factor 0.72 at $k = 0.1(\mathrm{km\,s^{-1}})^{-1}$ — almost precisely the suppression seen in the Figure, despite the non-linear transformation from optical depth to transmitted flux.

The dependence of $P_F(\mathbf{k})$ on $\gamma - 1$ is also simple to understand, through equation (9). Since $\tau \propto \Delta^\beta = (1 + \delta)^\beta$, with $\beta = 2 - 0.7(\gamma - 1)$, we expect that an increase in $\gamma - 1$ will decrease β and thus decrease the fluctuations in optical depth for given fluctuations in δ. A naive expansion assuming small δ predicts that the Lyα forest bias is proportional to β (Hui 1999; McDonald & Miralda-Escudé 1999) which would lead to a decrease in power by 17% for $2\delta(\gamma - 1) = 0.2$. The actual decrease in Figure 10(b) is less than half this prediction, which is reminiscent of the weaker than proportional dependence of the flux power on mass power. Note that the choice of $\Delta = 1.4$ for the normalization of the temperature-density relation appears to have the intended consequence of making the effective smoothing by thermal broadening mostly independent of $\gamma - 1$ (see McDonald et al. 2001).

The final parameter, $\bar{F}$, is varied by ± 0.025 in Figure 10(c) (black line with filled squares; $\bar{F}$ was actually varied by ± 0.05 in the simulations, so δP_F has been divided by 2). The decreasing power with increasing $\bar{F}$ is expected from the one-dimensional results of Croft et al. (1999) and McDonald et al. (2000). Fortunately for AP test purposes, the large-scale anisotropy does not depend sensitively on $\bar{F}$.

Now that we know how $P_F(\mathbf{k})$ depends on the parameters, at fixed redshift, it is interesting to see if we can treat a change in z as a simple rescaling of the parameters (as assumed by McDonald

et al. 2000). To create the red curve (with open squares) in Figure 10(c), I took outputs from the simulations at $z = 2.0$ and $z = 2.5$, instead of the usual $z = 2.25$. Both were analyzed using the usual values of $\bar{F}$, $T_{1.4}$, and $\gamma - 1$. Two obvious changes with redshift have been scaled away: The change in linear growth factor, approximately $\propto (1 + z)^{-1}$, can be treated as a change in power spectrum amplitude, A_1, so I have subtracted

$$\frac{dP_F}{dA_1} \frac{dA_1}{dz} \, 2\delta z \simeq \frac{\delta P_{F,A_1}}{2 \, \delta A_1} \left[\left(\frac{1 + 2.25}{1 + 2.5} \right)^2 - \left(\frac{1 + 2.25}{1 + 2.0} \right)^2 \right] A_1 \tag{23}$$

from the measured $\delta P_{F,z}$ (where I am using $\delta P_{F,p_i}$ to indicate the variation of P_F in the simulations with parameter p_i). A much less important term arising from the change in the temperature measured in comoving coordinates is also subtracted. The resulting curve shows that the parameter scaling approximation is close to perfect, except for a small deviation at the highest k. The primary remaining known error in the approximation is that the specified thermal history of the gas, which sets the pressure in the simulations, is offset by the difference in the two redshifts. The increase in power at high k might be explained by this if the effective smoothing scale is smaller than the Jeans scale, but increasing towards it over time, as predicted by Gnedin & Hui (1998).

In order to present these results in a quantitative, compact form that may be useful to others, I have fitted equation (20) to $P_F(\mathbf{k})$ for each of the parameter settings used in Figures 10(a,b,c). Table 1 lists the values of b_δ^2 and β for each variation of the model parameters, and the parameters of $D(\mathbf{k})$ for each fit. To save computer and organizational time, I do not recompute b_δ and b_η for each variation by the method in §3.4, because each b_δ requires the running of two extra simulations. Instead, the new values are set by solving ${b_\delta'}^2 = b_\delta^2 \, P_F'(k_{\min}, \mu = 0)/P_F(k_{\min}, \mu = 0)$, and ${b_\delta'}^2(1 + \beta')^2 = b_\delta^2(1+\beta)^2 \, P_F'(k_{\min}, \mu = 1)/P_F(k_{\min}, \mu = 1)$, where the unprimed quantities are at the central parameter values, and the primed are at the varied parameter values (considering the convergence tests in §3.4, this shortcut should be perfectly accurate). The agreement between the simulation results and the fitting results is good in all cases, in the sense that $\chi^2/\nu < 1$ using error bars computed as described in §3.5.

5. IMPLICATIONS FOR THE AP TEST

The primary motivation for computing $P_F(\mathbf{k})$ is to perform the AP test using the correlation between absorption in multiple lines of sight. McDonald & Miralda-Escudé (1999), and Hui, Stebbins, & Burles (1999) discussed using the Lyα forest AP test to measure Ω_Λ, and estimated the precision that could be obtained from hypothetical sets of data; however, these estimates were not based on any realistic calculation of the flux correlation, and did not address many of the relevant observational issues like the requirements on spectral resolution and signal-to-noise ratio. I can now do much better. Using my computed derivatives of $P_F(\mathbf{k})$ with respect to the model parameters, I can compute the Fisher information matrix for any hypothetical data set, and use it to find the smallest possible error bars on the parameters p_i, and the effects of different assumptions about

the data quality.

5.1. Lyα Forest Fisher Matrix

A very clear discussion of the Fisher information matrix and its uses can be found in Tegmark, Taylor, & Heavens (1997, see also references therein), here I only outline the essential points. If we represent a data set (i.e., a set of pixels in Lyα forest spectra) by the vector $\mathbf{x}$, and define the likelihood of observing $\mathbf{x}$ in a model with parameters $\mathbf{p}$ to be $L(\mathbf{x}; \mathbf{p})$, the Fisher matrix is

$$F_{ij} = -\left\langle \frac{\partial^2 \mathcal{L}}{\partial p_i \partial p_j} \right\rangle , \qquad (24)$$

where $\mathcal{L} = -\ln L$, and the $\langle ... \rangle$ brackets mean "average over all possible $\mathbf{x}$." If a maximum likelihood estimate is made of one parameter, p_i, with the others fixed, the rms error on p_i will be $1/F_{ii}^{-1/2}$. If the other parameters are marginalized over, the error bar on p_i is $(F^{-1})_{ii}^{1/2}$. One very useful fact about the Fisher matrix is that the error bars obtainable by combining multiple independent data sets can be estimated by simply adding up all the F's. Similarly, imposing a prior constraint, call it σ_i, on p_i is a simple matter of adding $1/\sigma_i^2$ to F_{ii}.

Calculating $L(\mathbf{x}; \mathbf{p})$ for the Lyα forest transmitted flux is in general difficult; however, for small enough k we expect that the Fourier modes will be independent and Gaussian, in which case $\mathcal{L}$ is given by

$$2\mathcal{L} = \ln \det \mathbf{C} + (\mathbf{x} - \mu)^T \mathbf{C}^{-1} (\mathbf{x} - \mu) + constant , \qquad (25)$$

where $\mu = \langle \mathbf{x} \rangle$ (not to be confused with $k_\parallel/k$), and $\mathbf{C} = \left\langle (\mathbf{x} - \mu)(\mathbf{x} - \mu)^T \right\rangle$, i.e., μ_i is the mean transmitted flux at pixel i, and C_{ij} is the correlation between pixel i and pixel j. The correlation between pixels is found from my computed $P_F(\mathbf{k})$ using equation (4). The effects of resolution and pixelization are included by convolving ξ_F with the appropriate window functions, and the mean squared noise level at pixel i is finally added to C_{ii}.

I have tested the validity of the assumption of independent Fourier modes by running many simulations with identical parameters, but different random initial conditions, and comparing the dispersion in the binned power spectrum measurements to error predictions made by assuming independent modes. By this test, the approximation appears to work well for $k \lesssim 2(h^{-1}\,\mathrm{Mpc})^{-1}$. I have done a preliminary check that the AP test using pairs with separations greater than a few arcminutes is primarily sensitive to power at $k \lesssim 2(h^{-1}\,\mathrm{Mpc})^{-1}$, so my Fisher matrix calculations should be reasonably accurate.

5.2. Application: SDSS Spectra

The SDSS will obtain spectra of ~ 100000 quasars, making the potential application of the Lyα forest AP test using this data very exciting. Fan (1999) gives predictions for the expected number

of quasars as a function of redshift and magnitude, which can be used to estimate the number of close pairs that will be found in the full 10000 square degrees of the survey. Assuming the planned limiting magnitude for obtaining spectra of $i' < 19.5^2$ (unfortunately, as I discuss below, this limit is not being reached), and counting only the Lyα forest region of spectra at $z \gtrsim 2.125$ (the cutoff below which the Lyα forest will not be observed), I estimate that SDSS would find overlapping regions of spectra equivalent to

$$N_{pair}(< \theta) \simeq 13 \left(\frac{\theta}{1'} \right)^2 \tag{26}$$

pairs with equal quasar redshifts and complete Lyα forest coverage, at separation less than θ (the actual number of partial pairs is of course larger than this). The mean redshift of the overlapping forest is $\bar{z} \simeq 2.35$.

For simplicity, the calculation that produced equation (26) assumed a random distribution of quasars, ignoring the increase in the number of pairs because of correlation. I estimate the effect of correlation by considering the number of quasars within transverse distance R from a given quasar, weighted by the fractional overlap of their Lyα forest spectra:

$$N(< R) = 2\pi \, \bar{n} \int_0^R r \, dr \int_{-z_{max}}^{z_{max}} \left(1 - \left| \frac{z}{z_{max}} \right| \right) \left[1 + \xi \left(\sqrt{r^2 + z^2} \right) \right] dz \ , \tag{27}$$

where $\bar{n}$ is the mean density of quasars, $z_{max} \sim 400 \, h^{-1}$ Mpc is the maximum overlap distance along the line of sight, and ξ is the correlation function. The fractional increase in pairs at a given separation due to correlation is given by

$$\frac{dN/dR}{dN_0/dR} - 1 = \frac{\int_0^{z_{max}} dz \, (1 - z/z_{max}) \, \xi \left(\sqrt{R^2 + z^2} \right)}{\int_0^{z_{max}} dz \, (1 - z/z_{max})} \ , \tag{28}$$

where N_0 is the uncorrelated case. Croom et al. (2001) measure the quasar correlation function from 2dF data and give results in terms of a power law $\xi(r) = (r/r_0)^{-\alpha}$. At $\bar{z} = 2.36$, they find $r_0 = 6.93^{+1.32}_{-1.64} \, h^{-1}$ Mpc and $\alpha = 1.64^{+0.29}_{-0.27}$ (assuming a flat universe with $\Omega_m = 0.3$). Evaluating equation (28) using the measured correlation, I find an increase of only 25% in the number of pairs at separation $R = 1 \, h^{-1}$ Mpc ($\theta \sim 1'$), which falls to 5% at $R = 10 \, h^{-1}$ Mpc. This difference is insignificant in the following discussion.

The SDSS signal-to-noise ratio for 1Å pixels is expected to be greater than 10 for a typical spectrum, with resolution 2000, or ~ 2Å FWHM at $z = 2.3$. For my first Fisher matrix calculation, I will assume that SDSS-quality spectra can be used off the shelf, i.e., I assume S/N=10, 1Å pixels, and resolution 2Å. Figure 11 shows basic results for the error bars on $f(z)$. (To make the results less abstract, I have translated the error on $f(z)$, $\Delta f(z)$, into an error on the cosmological constant, $\Delta \Omega_\Lambda \simeq 1.25 \, \Delta f$, by assuming $z = 2.25$, a flat universe, $\omega = -1$, and $\Omega_\Lambda \simeq 0.7$.) The squares show
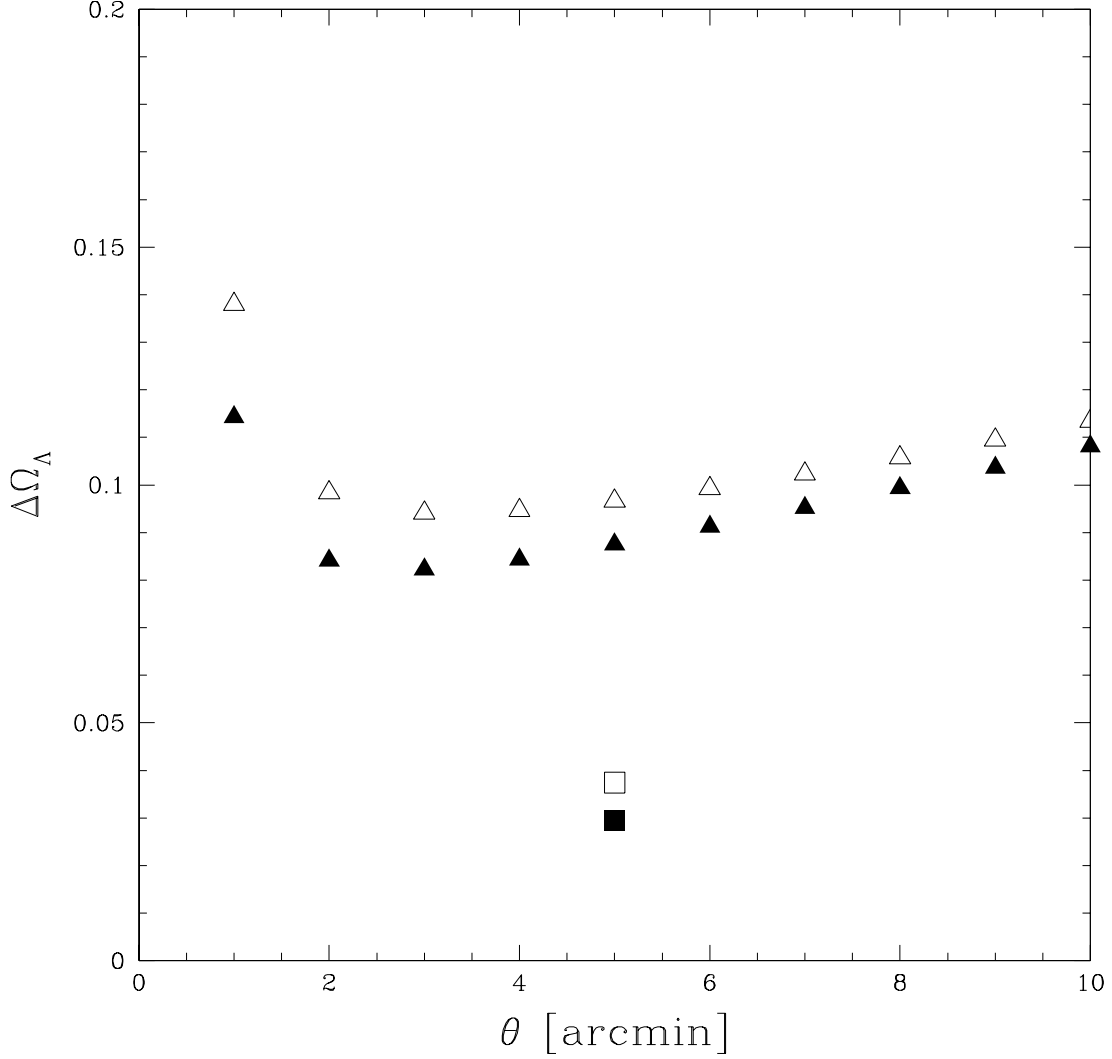
---

[2]http://www.sdss.org

Fig. 11.— Projected error bars on Ω_Λ from $N_{pair}(< \theta) = 13\,(\theta/1')^2$ fully overlapping spectra (for true value $\Omega_\Lambda \simeq 0.7$, and assuming $\omega = -1$ and $z = 2.25$). The triangles show the constraint using only pairs in each 1 arcminute interval of separations. The squares show the overall error, for $\theta < 10'$. The filled symbols assume that the parameters other than $f(z)$ are known, the open symbols assume they are marginalized over. In this, and the following figures, the horizontal positioning of the point showing the overall error is meaningless.

the estimated value of $\Delta\Omega_\Lambda$ obtained using all of the pairs with separation less than 10' (this cutoff is arbitrary, because the maximum separation, which will probably be set by quasar continuum issues, is unknown). To compute the solid square, I have assumed that the model parameters other than $f(z)$ ($\bar{F}$, $T_{1.4}$, $\gamma - 1$, A_1, and n_1) are known. This is not unreasonable because a huge number of single spectra will be available to constrain them. For the open square, I have marginalized over the other parameters assuming only the very weak constraints $\sigma_T = 4000$ K, $\sigma_{\gamma-1} = 0.3$, and $\sigma_{\bar{F}} = 0.03$. The triangles are the error projections for independent measurements of $f(z)$ made after splitting the pairs into groups by separation. Each triangle represents the constraint using only the pairs in a 1' interval of separations. The distinction between open and solid triangles is the same as for squares. This figure contains the primary result of this section: we can expect to measure Ω_Λ to ± 0.03 or ± 0.04 using $N_{pair}(< \theta) = 13 \, (\theta/1')^2$ fully overlapping, SDSS-quality spectra. As a consistency check, we can make measurements accurate to about ± 0.1 for each one arcminute interval of separations [$f(z)$ should not depend on θ]. The overall result is not very sensitive to pairs at small separations where some of my approximations will be least accurate.

Can we improve the measurement of $f(z)$ by taking spectra with better resolution or signal-to-noise ratio? Figure 12 shows the error estimates with S/N increased to 20 and 100. Improving S/N does not improve the overall results very much, helping most at small separations. Figure 13 shows the improvement with increased resolution. Again, the reduction in the error bars is greatest at small separations (not surprisingly), but does not improve the overall result very much.

Throughout this subsection, I have been assuming that the simulation predictions are essentially perfect, i.e., assuming that, given the input model parameters, I can compute the power spectrum exactly. It is informative to relax this assumption, by allowing for an error, $\Delta\beta$, in the predicted large-scale anisotropy parameter β. I treat β as a new free parameter in the Fisher matrix calculation, and plot in Figure 14 the resulting error in Ω_Λ as a function of the imposed constraint $\Delta\beta$. The solid line shows results using my usual set of pairs, and assuming only weak constraints on $\bar{F}$, $T_{1.4}$, and $\gamma - 1$. The precision of the Ω_Λ measurement is reduced from $\Delta\Omega_\Lambda = 0.037$ for perfectly predicted β, to $\Delta\Omega_\Lambda = 0.059$ if β is a completely free parameter. The transition between the two cases actually occurs at quite small values of $\Delta\beta/\beta$, because $\Delta\beta/\beta$ can be measured to 0.074 in a joint fit with $f(z)$. This result is a target for simulators to shoot at — predicting β to $\sim 7\%$ will allow a good consistency check, and improving the prediction further will improve the measurement of Ω_Λ. Finally, I show the results that can be obtained with only 10% of the usual data, as the dashed line. Ω_Λ can be constrained to almost ± 0.1 if a good prediction for β is available, and β can be measured to $\sim 17\%$ in a joint fit.

Unfortunately, as this paper was nearing completion, I discovered that the SDSS magnitude limit for obtaining spectra at $z < 3$ has slipped to $i' < 19.1$ (X. Fan, private communication), which will reduce the number of pairs by a factor of ~ 5 and correspondingly increase the errors by $5^{1/2}$. However, followup observations of pair candidates should be able to recover the level of precision I have discussed. Reducing the limit by another magnitude (to $i' < 20.5$) could increase the number of pairs by almost a factor of 10, giving a measurement of Ω_Λ to better than 2%!
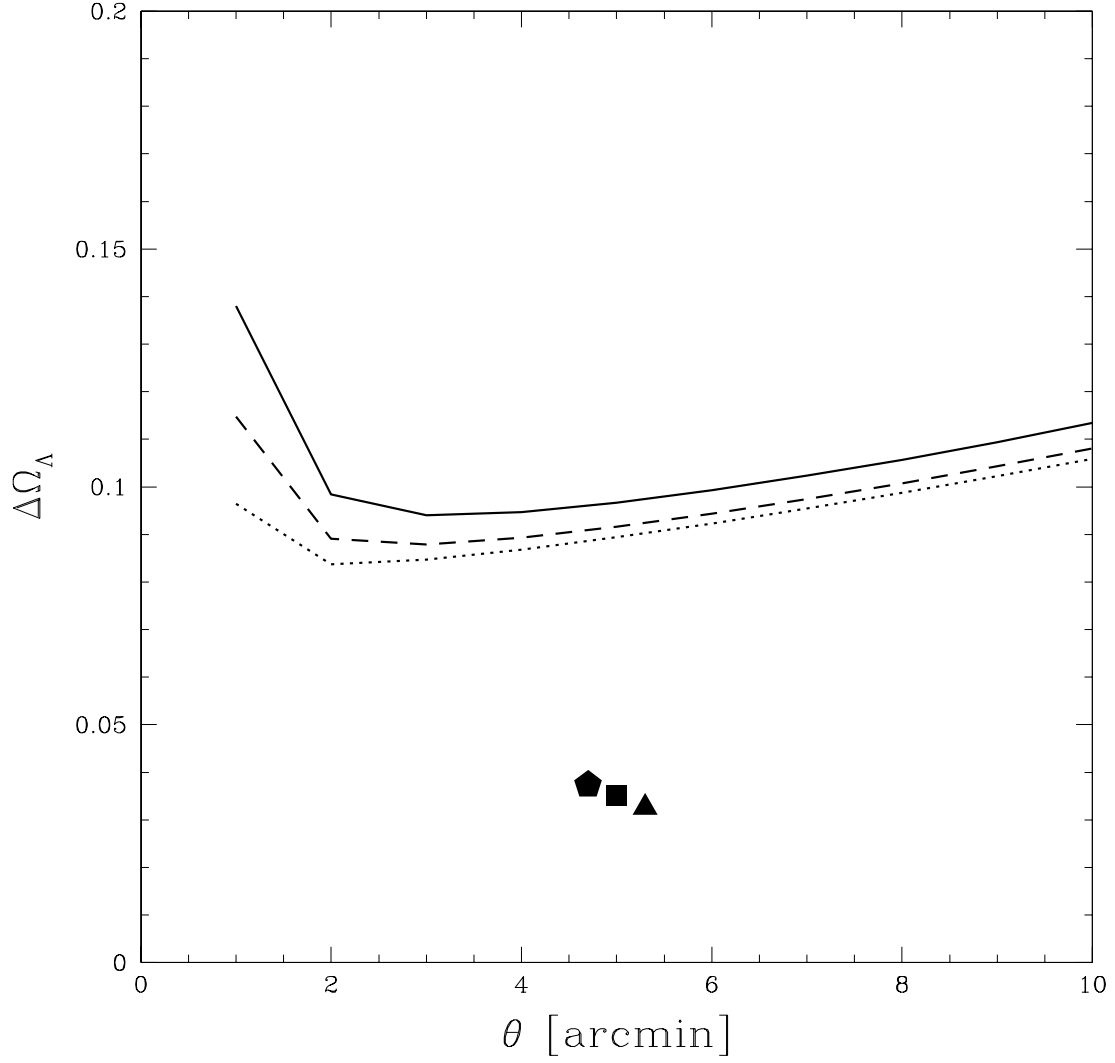
Fig. 12.— Sensitivity of error bars to noise level. The pentagon, square, and triangle represent S/N=10, 20, and 100, respectively, using all pairs with $\theta < 10'$, while the solid, dashed, and dotted lines show the error in 1' intervals for the same respective S/N.
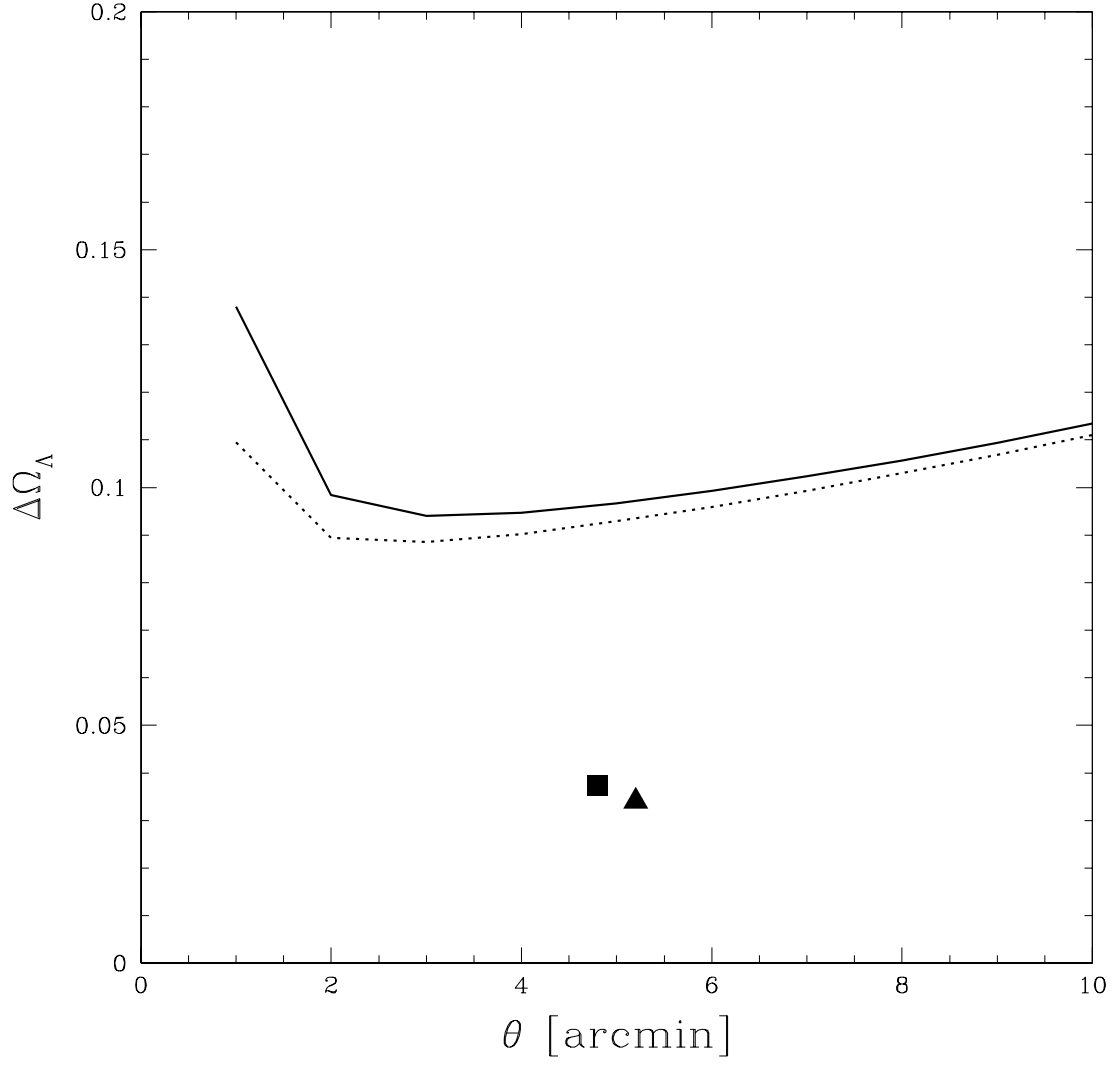
Fig. 13.— Sensitivity of error bars to resolution. The solid line and the square show resolution 2 Å. The dotted line and triangle show 1 Å. Resolutions are FWHM, with pixel sizes 1Å and 0.5Å, respectively.
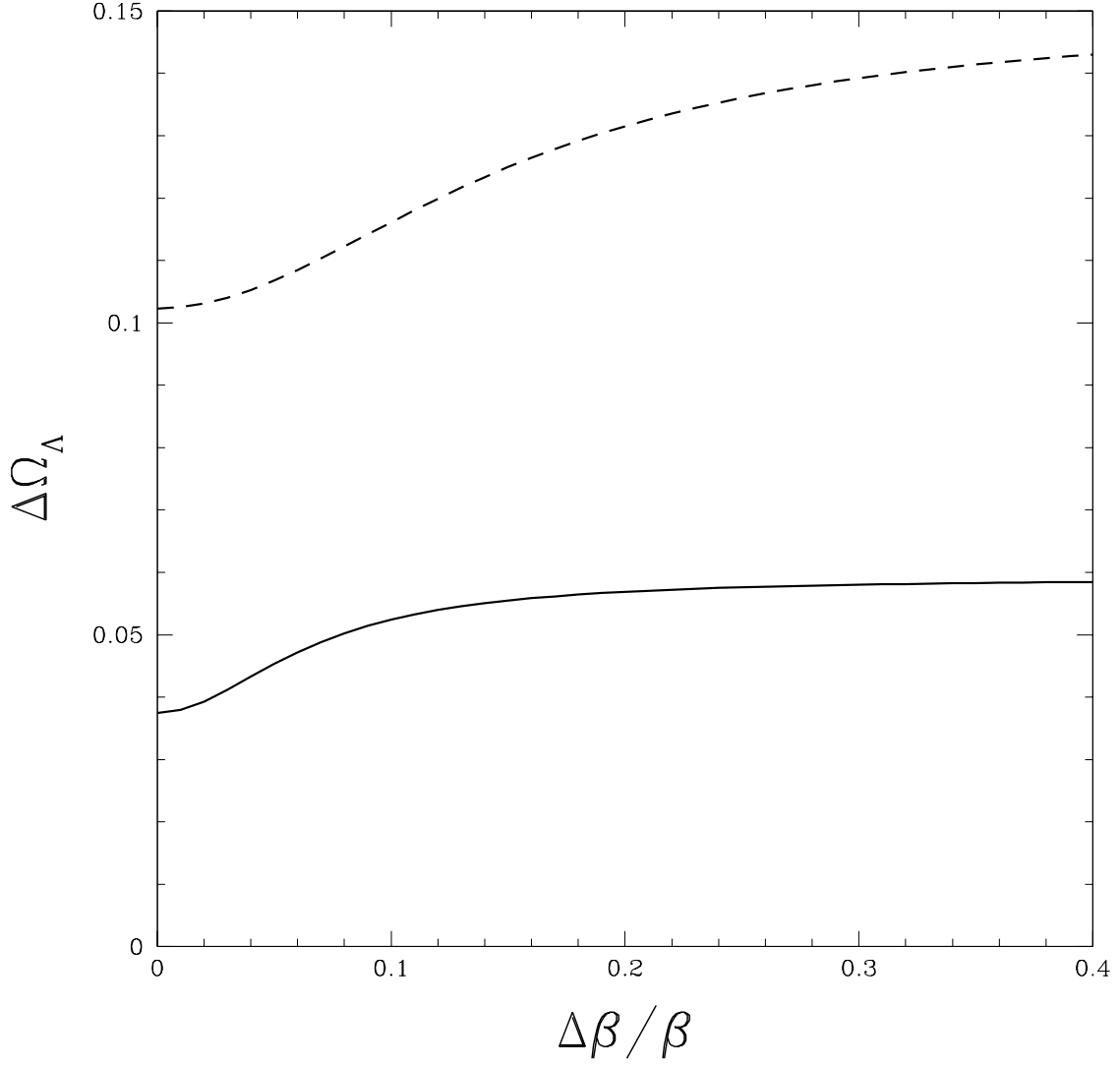
Fig. 14.— Sensitivity of error bars to accuracy of the power spectrum anisotropy predictions. The solid line shows the constraint on Ω_Λ as a function of the theoretical error on β, using $N_{pair}(<\theta) = 13\,(\theta/1')^2$ full pairs. The dashed line shows the same thing for 10% of the data.

6. CONCLUSIONS

I have computed the three-dimensional power spectrum of the transmitted flux, $P_F(\mathbf{k})$, using Hydro-PM (HPM) simulations. From $P_F(\mathbf{k})$, we can calculate the correlation between absorption in the spectra of close pairs of quasars. The results for $P_F(\mathbf{k})$ for a set of model parameter variations are given in Table 1, in terms of the parameters of equation (20).

I have investigated the importance of pressure, resolution, and box size in the simulations. Figure 5 shows that the pressure force in the HPM simulations has an effect no larger than $\sim 10\%$ on the large-scale power (relative to no pressure at all), but as much as $\sim 40\%$ on small scales. However, within the HPM approximation, the change in pressure corresponding to a ~ 4000 K change in temperature results in $\lesssim 2\%$ change in power at all relevant k, so it is not important to know the detailed thermal history of the gas in order to compute the pressure. Figure 6(a,b) shows that the required resolution for convergence of the power (to $\sim 5\%$) on all relevant scales is $\sim 40\,h^{-1}\,\mathrm{kpc}$, while $80\,h^{-1}\,\mathrm{kpc}$ gives good results for $k \lesssim 1 - 2(\,h^{-1}\,\mathrm{Mpc})^{-1}$ only, and $160\,h^{-1}\,\mathrm{kpc}$ gives poor results on all scales. Figure 7 shows that box size $L \sim 40\,h^{-1}\,\mathrm{Mpc}$ is required for convergence of the small-scale power, while reducing the box size to $L = 20\,h^{-1}\,\mathrm{Mpc}$ leads to extra power along the line of sight. My calculation of the large-scale bias in §3.4 shows that $40\,h^{-1}\,\mathrm{Mpc}$ simulations are sufficiently large for this purpose also. Future simulation work will be focused on determining the accuracy of the HPM approximations, and running larger simulations.

One of the primary reasons to measure the correlation between the Lyα forest absorption in multiple lines of sight is to determine the cosmological geometry through the Alcock & Paczyński (1979) test (McDonald & Miralda-Escudé 1999; Hui, Stebbins, & Burles 1999), which I show can break the degeneracy between matter and vacuum energy in a flat universe (see Figure 2), in a way that is *independent of the equation of state of the vacuum energy* (Figure 3). I used my results for $P_F(\mathbf{k})$ to estimate the constraining power of the AP test performed using future data sets. Figures 11 and 14 show that, using $N_{pair}(< \theta) = 13\,(\theta/1')^2$ fully overlapping pairs of spectra at angular separation $< \theta$, with $\theta < 10'$, Ω_Λ can be measured to between ± 0.03 and ± 0.06, depending on our ability to accurately measure or calculate other parameters of the Lyα forest model. The Sloan Digital Sky Survey will only obtain spectra for a factor of ~ 5 fewer pairs than this, but followup observations of pair candidates to magnitude $i' < 19.5$ should be able to achieve the results discussed. Figures 12 and 13 show that only small gains are obtainable by improving spectral quality beyond SDSS's signal-to-noise ratio, $S/N > 10$ (for 1 Å pixels), and resolution, 2 Å (FWHM).

The results in this paper should have a wide variety of applications. For example, the power spectrum calculations should be sufficiently accurate for comparison with a data set consisting of all the currently known pairs (to be safe, $P_F(\mathbf{k})$ in this paper should not be trusted if better than 20% accuracy is important, although it may be more accurate than this). They will also be useful for planning future observing programs. The power of the Lyα forest AP test in combination with other measurements of cosmological parameters can be investigated. Furthermore, other uses of the Lyα forest to constrain cosmology can be explored using a realistic power spectrum, e.g., using the

very large quasar surveys to essentially measure $P_F(\mathbf{k})$ directly on very large scales (larger than the mean transverse quasar separation), and constrain the detailed shape of the primordial mass power spectrum [i.e., possibly measuring $\Gamma(z) \equiv \Omega_m h^2 (1+z)/H(z)$, or even detecting baryonic wiggles]. The computed bias parameters relating large-scale fluctuations in the Lyα forest to fluctuations in the mass can be used to interpret correlations between the Lyα forest and other observables, such as Lyman-break galaxies. Finally, this paper should provide a useful starting point for future simulation projects that seek to compute $P_F(\mathbf{k})$ more accurately.

REFERENCES

Alcock, C. & Paczyński, B. 1979, Nature, 281, 358

Balbi, A. et al. 2000, ApJ, 545, L1

Bechtold, J., Crotts, A. P. S., Duncan, R. C., & Fang, Y. 1994, ApJ, 437, L83

Benson, A. J., Cole, S., Frenk, C. S., Baugh, C. M., & Lacey, C. G. 2000, MNRAS, 311, 793

Bi, H. G. 1993, ApJ, 405, 479

Blanton, M., Cen, R., Ostriker, J. P., & Strauss, M. A. 2000, ApJ, 531, 1

Cen, R., Miralda-Escudé, J., Ostriker, J. P., & Rauch, M. 1994, ApJ, 437, L9

Cen, R. & Ostriker, J. P. 2000, ApJ, 538, 83

Croft, R. A. C., Weinberg, D. H., Bolte, M., Burles, S., Hernquist, L., Katz, N., Kirkman, D., & Tytler, D. 2000, ApJ, submitted (astro-ph/0012324)

Croft, R. A. C., Weinberg, D. H., Katz, N., & Hernquist, L. 1997, ApJ, 488, 532

Croft, R. A. C., Weinberg, D. H., Pettini, M., Hernquist, L., & Katz, N. 1999, ApJ, 520, 1

Crotts, A. P. S., & Fang, Y. 1998, ApJ, 502, 16

Davé, R., Hernquist, L., Weinberg, D. H., & Katz, N. 1997, ApJ, 477, 21

de Bernardis, P. et al. 2000, Nature, 404, 955

Dinshaw, N., Impey, C. D., Foltz, C. B., Weymann, R. J., & Chaffee, F. H. 1994, ApJ, 437, L87

Eisenstein, D. J., Hu, W., & Tegmark, M. 1999, 518, 2

Fan, X. 1999, AJ, 117, 2528

Gnedin, N. Y. 1998, MNRAS, 299, 392

Gnedin, N. Y. & Hui, L. 1998, MNRAS, 296, 44

Hamilton A. J. S. & Tegmark M. 2000, MNRAS, submitted (astro-ph/0008392)

Hernquist, L., Katz, N., Weinberg, D. H., & Miralda-Escudé, J. 1996, ApJ, 457, L51

Hui, L. 1999, ApJ, 516, 519

Hui, L., Gnedin, N. Y., Zhang, Y. 1997, ApJ, 486, 599

Hui, L., Stebbins, A., & Burles, S. 1999, ApJ, 511, L5

Hui, L., Burles, S., Seljak, U., Rutledge, R. Magnier, E., Tytler, D. 2001, ApJ, 552, 15

Hui, L. & Gnedin, N. 1997, NMRAS, 292, 27

Huterer, D. & Turner, M. S. 2001, Phys. Rev. D, submitted (astro-ph/0012510)

Kaiser, N. 1987, MNRAS, 227, 1

Ma, C.-P. 1998, ApJ, 508, L5

McDonald, P. & Miralda-Escudé, J. 1999, ApJ, 518, 24

McDonald, P. & Miralda-Escudé, J. 2001, ApJ, 549, L11

McDonald, P., Miralda-Escudé, J., Rauch, M., Sargent, W. L. W., Barlow, T. A., Cen, R., & Ostriker, J. P. 2000, ApJ, 543, 1

McDonald, P., Miralda-Escudé, J., Rauch, M., Sargent, W. L. W., Barlow, T. A., & Cen, R. 2001, ApJ, in press (astro-ph/0005553)

McGill, C. 1990, MNRAS, 242, 544

Meiksin, A. & White, M. 2001, MNRAS, 324, 141

Miralda-Escudé, J., Cen, R., Ostriker, J. P., & Rauch, M. 1996, ApJ, 471, 582

Petitjean, P., Mücket, J. P., & Kates, R. E. 1995, A&A, 295, L9

Rauch, M., Miralda-Escudé, J., Sargent, W. L. W., Barlow, T. A., Weinberg, D. H., Hernquist, L., Katz, N., Cen, R., & Ostriker, J. P. 1997, ApJ, 489, 7

Ricotti, M., Gnedin, N. Y., & Shull, J. M. 2000, ApJ, 534, 41

Somerville, R. S., Lemson, G., Sigad, Y., Dekel, A., Kauffmann, G., White, S. D. M. 2001, MNRAS, 320, 289

Tegmark, M., Taylor, A. N., & Heavens, A. F. 1997, ApJ, 480, 22

Tegmark, M. & Zaldarriaga, M. 2000, Phys. Rev. Lett., 85, 2240

Theuns, T., Leonard, A., Efstathiou, G., Pearce, F. R., & Thomas, P. A. 1998, MNRAS, 301, 478

Theuns, T., Leonard, A., Schaye, J., & Efstathiou 1999, MNRAS, 303, L58

Weinberg, D. H., Katz, N., & Hernquist, L. 1998, in ASP Conference Series 148, Origins, eds. C. E. Woodward, J. M. Shull, & H. Thronson, (ASP: San Francisco), 21 (astro-ph/9708213)

York, D. G. et al. 2000, AJ, 120, 1579

Zaldarriaga, M., Hui, L., & Tegmark, M. 2000, ApJ, submitted (astro-ph/0011559)

Zaldarriaga, M., Seljak, U., & Hui, L. 2001, ApJ, 551, 48

Zhang, Y., Anninos, P., & Norman, M. L. 1995, ApJ, 453, L57

Table 1.   Power Spectrum Results

$\delta\mathbf{p}$	b_δ^2	β	k_{NL}	α_{NL}	k_P	α_P	k_{V0}	α_V	k_V'	α_V'
0	0.0173	1.58	6.40	0.569	15.3	2.01	1.220	1.50	0.923	0.451
$+\delta A_1$	0.0151	1.66	6.59	0.524	16.0	2.11	0.963	1.50	0.727	0.487
$-\delta A_1$	0.0197	1.51	6.30	0.568	15.2	1.94	1.430	1.50	0.843	0.391
$+\delta n_1$	0.0171	1.62	8.30	0.551	16.0	2.05	1.183	1.48	0.920	0.447
$-\delta n_1$	0.0175	1.54	5.07	0.579	14.5	1.94	1.254	1.53	0.929	0.456
$+\delta T_{1.4}$	0.0173	1.58	6.41	0.571	15.2	2.01	1.205	1.51	0.829	0.431
$-\delta T_{1.4}$	0.0173	1.58	6.42	0.570	15.3	2.00	1.234	1.50	1.025	0.473
$+\delta(\gamma-1)$	0.0171	1.57	6.42	0.568	15.2	2.03	1.242	1.48	0.959	0.443
$-\delta(\gamma-1)$	0.0176	1.59	6.39	0.576	15.2	1.97	1.196	1.53	0.885	0.459
$+\delta\bar{F}$	0.0126	1.49	5.21	0.707	13.1	1.83	1.476	1.43	2.135	0.469
$-\delta\bar{F}$	0.0235	1.66	5.62	0.613	12.6	1.70	0.895	1.54	0.431	0.464

Note. — k's measured in $(h^{-1}\,\mathrm{Mpc})^{-1}$. $\delta A_1 = 0.29$, $\delta n_1 = 0.1$ (at fixed σ_1), $\delta T_{1.4} = 2000$ K, $\delta(\gamma-1) = 0.05$, and $\delta\bar{F} = 0.05$.